mater.scichina.com link.springer.com

Published online 8 September 2022 | https://doi.org/10.1007/s40843-022-2153-7
Sci China Mater 2022, 65(11): 2911–2935

Recent advance in three-dimensional porous carbon materials for electromagnetic wave absorption

Mingrui Han[1], Yunfei Yang[1], Wei Liu[2], Zhihui Zeng[1*] and Jiurong Liu[1*]

ABSTRACT With the increasingly serious electromagnetic wave (EMW) pollution, the development of high-performance EMW absorbing materials (EWAMs) has become a hot topic. Carbon-based EWAMs have excellent chemical stability, high electrical conductivity, and strong dielectric loss. In particular, three-dimensional (3D) porous carbon-based EWAMs have been widely developed in the EMW absorption field. The 3D porous structure not only reduces the materials' mass density, but also improves the multiple reflections of incident EMWs and impedance matching. The carbon-based EWAMs are thus expected to achieve the goals of low density, low thickness, wide absorption bandwidth, and strong absorption. Herein, we first restated the relevant theoretical basis and evaluation methods. Then, we summarized the recent research progress of 3D porous carbon-based EWAMs with the source of the materials as the main clue. Some unique and novel viewpoints were highlighted. Finally, the challenges and prospects of 3D porous carbon-based EWAMs were put forward, which is helpful for guiding a further development of high-performance EWAMs.

Keywords: carbon materials, porous, electromagnetic wave absorption, reflection loss, impedance matching

INTRODUCTION

With the development of communication technology and electronic equipment in recent years, electromagnetic wave (EMW) interference and pollution have become more and more serious. EMWs can interfere with the normal operation of highly sensitive electronic devices [1–4], and even affect the physical health [5,6]. In the military field, radar stealth coatings made of EMW absorbing materials (EWAMs) effectively improve the concealment and battlefield survivability of fighter planes, tanks, and warships. In addition, EWAMs can convert the absorbed electromagnetic energy [7,8], which endows them with great potential in the sensing field. Especially with the advent of the era of intelligence, EWAMs were also expected to show their cutting edge in wearable devices [9], electromagnetic sensing [10], energy conversion [11,12], etc. Therefore, there is an urgent need to develop high-performance EWAMs, which can not only prevent the harm of EMWs to human body and electronic devices, but also realize the stealth of military equipment and promote the progress of novel sensors.

According to the loss type, EWAMs can be divided into two categories: the magnetic-loss materials such as ferrite [13–15], and the dielectric-loss materials, including metal oxides [16–18], metal sulfides [19–21], carbides [22–24], and carbon materials [25–27]. Carbon materials, such as carbon nanotubes (CNTs) [28,29], graphene [30,31], graphene aerogels (GAs) [32,33], and biomass carbon (BC) [34,35], have great potentials to be excellent absorbers due to their good mechanical properties, chemical stability, and not least in terms of high electrical conductivity [36,37]. Naturally, the development of carbon-based EWAMs has become a hot spot of the current research.

Three-dimensional (3D) porous materials have attracted increasing attention due to many unique superiorities. Particularly, 3D porous carbon materials have diverse microscopic morphologies, which have an influence on the EMW absorbing performance. The 3D porous carbon materials generally have low density and large specific surface area. The synergy of abundant pores and interconnected carbon frameworks can optimize the impedance matching and induce multiple reflections of incident EMWs, enhancing the EMW absorbing performance of the carbon-based absorbers. Previous reports have shown that the carbon materials with 3D porous structure showed excellent EMW absorbing performance [38–40]. However, in consideration of the varieties of 3D porous carbon materials, the influences of the material source and structure on the EMW absorbing performance are worthy of more attention. As for material sources, different processing technologies and chemical compositions may lead to different intrinsic electromagnetic properties of the materials. For 3D porous architectures, larger and denser pores will bring about larger internal spaces, which are conducive to the impedance matching and multiple reflections of incident EMWs, but excessive pore volume and density can cause the structure to be fragile and transparent to EMWs. Thus, to achieve a strong EMW absorption, the size and density of pores need to be comprehensively traded off. In addition, the opening or closing of the pore is also a factor to consider, which affects the reflection and refraction of the EMWs. Accordingly, it is necessary to review and sort the current research of the 3D porous carbon-based EWAMs. Herein, recent progress in 3D porous carbon-based EWAMs was summarized, and the performance of different materials was also compared. We anticipate that some ideas or

[1] Key Laboratory for Liquid-Solid Structural Evolution and Processing of Materials, Ministry of Education and School of Materials Science and Engineering, Shandong University, Jinan 250061, China
[2] State Key Laboratory of Crystal Materials, Shandong University, Jinan 250100, China
[*] Corresponding authors (emails: zhihui.zeng@sdu.edu.cn (Zeng Z); jrliu@sdu.edu.cn (Liu J))

inspirations can be provided for subsequent research.

EMW ABSORPTION THEORY AND DESIGN PRINCIPLES OF EMAWs

EMW absorption theory

To achieve EMW absorption, two requirements need to be met: (1) instead of being reflected, EMWs should enter into EWAMs as much as possible, namely, achieving impedance matching is vital. (2) EWAMs should possess potent EMW attenuation capability, so that the energy of incident EMWs can be converted into various forms of energy to dissipate as much as possible.

EMWs are reflected and transmitted when they radiate to the EWAMs from free space. According to the transmission line theory, the input impedance of the absorbers (Z_{in}) can be expressed as [41–43]

$$Z_{in} = Z_0\left(\frac{\mu_r}{\varepsilon_r}\right)^{1/2}\tanh\left[j\frac{2\pi fd}{c}(\varepsilon_r\mu_r)^{1/2}\right], \quad (1)$$

where Z_0 is the free space impedance, ε_r ($\varepsilon_r = \varepsilon' - j\varepsilon''$), μ_r ($\mu_r = \mu' - j\mu''$), and d are the complex permittivity, complex permeability, and thickness of the absorbers, respectively, f and c represent the frequency of EMWs and the speed of light, respectively. The reflection coefficient (R) of EMWs on the surface of absorbers can be described as

$$R = \frac{Z_{in} - Z_0}{Z_{in} + Z_0}. \quad (2)$$

Theoretically, when $Z_{in} = Z_0$, R is equal to 0, which means that EMWs can all enter the interior of the EWAMs, which is called "impedance matching". Since Z_{in} and Z_0 cannot keep consistent in both real and imaginary parts, $|Z_{in}/Z_0| = 1$ was used as a convenient and universal criterion to evaluate the impedance matching in some cases.

When EMWs enter the absorbers, they will be attenuated by some mechanisms. These electromagnetic energy loss mechanisms can be divided into three types: magnetic loss, polarization loss, and conductive loss. Magnetic loss is described as the characteristic magnetic interaction between incident EMWs and absorbers, which mainly includes domain wall resonance loss, hysteresis loss, eddy current loss, exchange resonance and natural resonance. Natural resonance and eddy current loss are the main forms of magnetic loss at gigahertz frequencies. The essence of natural resonances is the damping motion of the magnetic moment around the magnetic anisotropy field. The relationship between natural resonance and anisotropy field can be described as [44]

$$f_r = \frac{\gamma H_\alpha}{2\pi}, \quad (3)$$

where f_r stands for the natural resonance frequency, H_α is the anisotropy energy, and γ is the gyromagnetic ratio. Eddy current, which is generated by electromagnetic induction, flows inside the magnetic conductor and thus dissipates the electromagnetic energy. C_0 is usually used to evaluate the contribution of eddy currents to the EMW attenuation [45]:

$$C_0 = \mu''(\mu')^{-2}f^{-1} = 2\pi\sigma\mu_0 d^2, \quad (4)$$

where μ_0 is the permeability of free spaces, and σ refers to the conductivity of the material. When C_0 is expressed as a constant, the magnetic loss is thought to primarily derive from eddy current loss.

Polarization loss is the attenuation of electromagnetic energy caused by the lossy polarization relaxation process, which mainly exists in the mediums with very low conductivity and on the hetero interfaces. According to the Debye theory, if the conductivity is negligible, the ε' and ε'' will satisfy the following equation [46]:

$$\left(\varepsilon' - \frac{\varepsilon_s + \varepsilon_\infty}{2}\right)^2 + (\varepsilon'')^2 = \left(\frac{\varepsilon_s - \varepsilon_\infty}{2}\right)^2, \quad (5)$$

where ε_s is the static permittivity, and ε_∞ represents the permittivity at high frequency limit.

Conductive loss is caused by the Joule heating effect of the induced current formed by free electrons under the action of a magnetic field. According to the free electron theory, the dependence of ε'' and σ for high conductivity materials can be described as [47]

$$\varepsilon'' \approx \frac{\sigma}{2\pi\varepsilon_0 f}, \quad (6)$$

where ε_0 stands for the permittivity of vacuum.

For qualitative analysis, Cole-Cole plots reflect the relationship between ε' and ε''. Thus, each polarization loss behavior is shown as a semi-circle in the Cole-Cole plots, while the conductive loss behavior is shown as an upwardly raised "tail" in the low frequency region. For quantitative analysis, ε'' needs to be separated to dissect the contribution of polarization loss and conductive loss [48,49]. The corresponding equation is shown as follows:

$$\varepsilon'' = \varepsilon_p'' + \varepsilon_c'', \quad (7)$$

where ε_p'' and ε_c'' represent the polarization and conduction components of the imaginary part of the dielectric constant respectively. ε_c'' can be calculated by Equation (6), so when ε'' is measured, ε_p'' is obtained.

What is more, based on the transmission line theory and metal backplane model (Fig. 1), the attenuation factor α, which reflects the EMW attenuation capability of EWAMs, can be calculated by the following equation [36,50]:

$$\alpha = \frac{\sqrt{2}\pi f}{c} \times \sqrt{\mu''\varepsilon'' - \mu'\varepsilon' + \sqrt{(\mu''\varepsilon'' - \mu'\varepsilon')^2 + (\mu'\varepsilon'' + \mu''\varepsilon')^2}}. \quad (8)$$

It can be seen that the impedance matching and EMW attenuation characteristic of EWAMs are both related to the electromagnetic parameters (ε_r and μ_r) [51,52]. Therefore, to achieve excellent EMW absorbing performance, reasonable

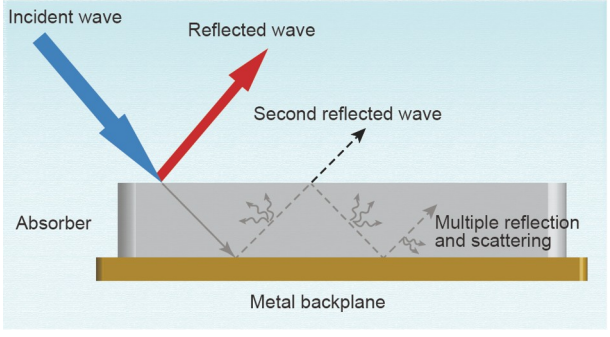

Figure 1 Propagation of EMWs in EWAMs.

electromagnetic parameters are demanded for EWAMs. Generally, the EMW absorbing performance of EWAMs is evaluated by the minimum reflection loss (RL_{min}) and effective absorption bandwidth (EAB). Based on the transmission line theory, the reflection loss (RL) can be expressed as the following equation [53,54]:

$$RL = 20\log\left|\frac{Z_{in}-Z_0}{Z_{in}+Z_0}\right|. \quad (9)$$

The value of RL less than −10 dB means that more than 90% of the incident EMWs will be absorbed. The width of the frequency band with RL < −10 dB under a certain thickness is called EAB. RL_{min} and EAB reflect the absorption strength and the coverage of absorption capacity of EWAMs, respectively. Therefore, low RL_{min} and broad EAB become constant pursuit for achieving highly efficient EWAMs.

Design principles of carbon-based materials

For carbon-based EWAMs, they possess huge advantages in terms of density and electrical conductivity. However, high conductivity tends to cause high dielectric constant, and in turn causes mismatched impedance [36,55], which hinders the EMW absorption performance. In current studies, the modifications on carbon-based EWAMs are mainly carried out from three aspects.

(1) Conductivity adjustment of carbon materials. The high electrical conductivity of carbon materials is a "double-edged sword". According to the free electron theory, the high conductivity enhances the dielectric loss ability of absorbers and promotes the consumption of incident EMWs. Nevertheless, excessively high conductivity causes the strong reflection of EMWs on the surface of absorbers. Therefore, optimizing the electrical conductivity is an essential way to improve the EMW absorbing performance of carbon materials. For example, good impedance matching can be achieved by reducing the conductivity of reduced graphene oxide (rGO) through heteroatom doping or introducing defects, which enables rGO to achieve optimized EMW absorbing performance [56].

(2) Morphology design of carbon materials. The microstructure has a significant influence on EMW absorption properties of carbon materials. Previous studies have shown that 3D porous carbon materials can form massive electron conducting networks, increasing conductive loss [57,58]. Meanwhile, the porous structure increases the multiple reflections or scatterings of the incident EMWs and reduces the density of the materials. Moreover, according to the Maxwell-Garnett theory [59], 3D porous carbon materials with adjustable pore structures are beneficial for the simple modulation of the dielectric constant to achieve good impedance matching.

(3) Composites of carbon materials and other materials. In terms of composites, not only the high dielectric constant can be effectively optimized, but also the introduced multiple losses effectively can increase the EMW loss ability. For instance, when carbon materials are integrated with magnetic materials, the composites can provide additional magnetic loss and then realize the optimization of impedance matching by the improved magnetic permeability [60,61].

In conclusion, although there are still formidable challenges to develop carbon-based EWAMs with ideal EMW absorbing performance, some design principles of carbon-based EWAMs are very clear, that is, carbon-based EWAMs oriented towards 3D porous structure and material compositing are expected to achieve excellent EMW absorbing performance. Herein, the recent research progress of 3D porous carbon-based and composite EWAMs will be introduced in the following part.

3D POROUS CARBON MTERIALS FOR EMW ABSORPTION

3D graphene-based materials

Graphene has received extensive attention due to its excellent electrical conductivity, low density, and large theoretical specific surface area (~2628.8 $m^2 g^{-1}$). Especially, the rGO possesses abundant defects and hydroxyl, epoxy, and carboxyl groups, which may provide considerable dielectric loss [62]. Considering the conductive loss caused by good electrical conductivity as well as the polarization loss caused by abundant defects and functional groups, graphene may be a very competitive dielectric loss material. However, the van der Waals force between graphene layers causes the inevitable stacking of monolithic graphene. Whether the stacking of graphene has any effect on its EMW absorbing performance is still inconclusive. In general, the EMW absorbing performance of 2D graphene materials is unsatisfactory due to the mismatched impedance derived from the excessively high conductivity. Fortunately, the graphene-based absorbers with 3D porous structures may solve the above issue since lots of air filled in pores can efficiently optimize the impedance matching, which rekindles the hope of graphene-based materials in the field of EMW absorption.

3D pure graphene materials

Pure 3D carbon materials may still be criticized for the high electrical conductivity resulting in impedance mismatch. The electrical conductivity can directly affect the imaginary part of permittivity (ε'') [55], and then determines the EMW absorption of materials. Previous studies reported that the heat treatment could modulate the reflection/absorption mechanisms [63]. The rGO aerogels with different reduction states were obtained by adjusting the heat treatment temperature. As the annealing temperature increases, the electrical conductivity enhances, and the electromagnetic mechanism gradually changes from absorption to reflection (Fig. 2a). Therefore, it is crucial to optimize the EMW absorption capacity of carbon materials by adjusting the electrical conductivity, which has also been considered in recent studies. As shown in Fig. 2c, Liu *et al.* [64] developed a self-assembly hydrothermal approach to fabricate N-doped graphene foams (NGF) with an open reticular structure. Pyrrolic/pyridinic N contributed to dipolar relaxation loss, while graphitic N led to enhanced electrical conductivity, increasing the conductive loss. Moreover, 3D interconnected conductive network provided more transport routes for electrons. Compared with conventional 2D materials, apart from the electron migration on a single graphene sheet, there is also electron hopping among adjacent graphene sheets in 3D structure, which increases the conductive loss of the material (Fig. 2d). Consequently, NGF displayed the RL_{min} of −53.9 dB with the filler loading as low as 5 wt%, and the corresponding EAB was 4.56 GHz (Fig. 2b). Usually, graphene has excellent in-plane conductivity. The electron conduction between the graphene sheets is also not negligible in 3D structure. However, electron hopping between graphene sheets is limited by weak van der Waals forces between sheets and strong electrostatic

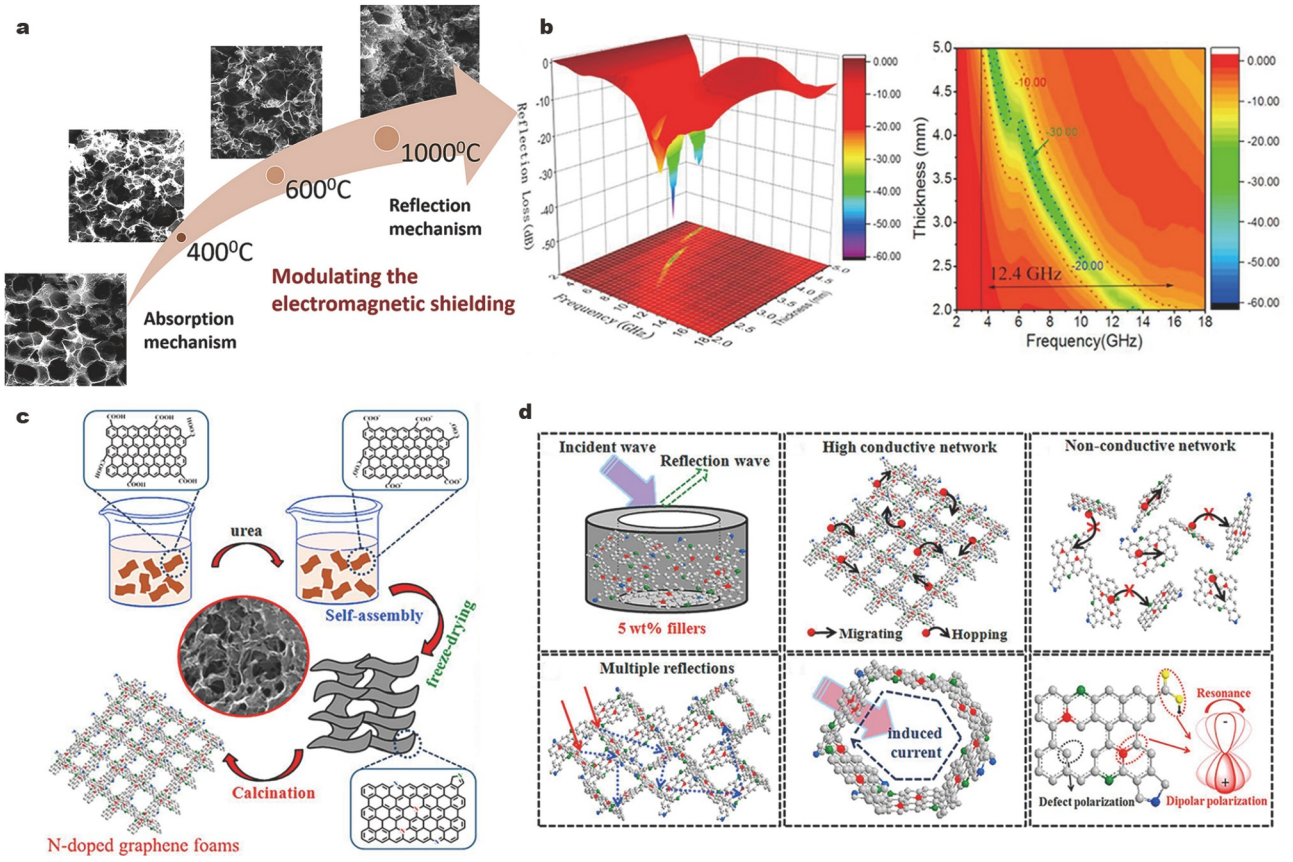

Figure 2 (a) Schematic illustration of the relationship between the annealing temperature and absorption/reflection behavior. Reprinted with permission from Ref. [63]. Copyright 2019, Elsevier. (b–d) EMW absorption performance, preparation process, and EMW absorption mechanisms of the NGF. Reprinted with permission from Ref. [64]. Copyright 2019, Elsevier.

repulsion from oxygen-containing functional groups. Liu and her coworkers [65] proposed to weaken the inter-sheet electrostatic repulsion arose from negatively charged oxygen-containing functional groups by introducing I^+, which strengthened the interconnection of rGO sheets and further improved the vertical conductivity of stacked rGO sheets. Thanks to enhanced electrical conductivity, I^+ modulated rGO aerogel (3D rGO-I) demonstrated an optimum RL_{min} of −52.8 dB with an EAB of 6.8 GHz at 2 wt% filler loading.

Apart from the adjustment of conductivity, researchers have also put forward new insights into the morphology design of graphene materials. As for macroscopic morphology, Meng and his coworkers [66] explored the tailorable manipulation and scalable fabrication of GA. They prepared GA spheres with controlled hollow structures (HGAS) and ball-in-ball GA spheres (BGAS) by triaxial electrospinning (Fig. 3a–c). Hollow structure effectively optimized the impedance matching. The HGAS sample showed an RL_{min} of −52.7 dB with a thickness of 2.3 mm and a broad EAB of 7.0 GHz. Meanwhile, the BGAS sample could reach an outstanding EAB of 9.3 GHz. The authors attributed these impressive EMW absorption capabilities to 3D interconnected graphene networks. The formation of 3D graphene networks increased the specific surface area and provided sufficient electron transport pathways, facilitating the attenuation of EMWs (Fig. 3d). Sun *et al.* [67] explored the relationship between the shape of rGO aerogel and EMW absorption performance at the centimeter scale through experiments and simulations. Sphere (GS-s), cubic (GS-c), hexagonal prism (GS-hp) and frustum pyramid (GS-fp) were fabricated by injecting the GO aqueous solution into the corresponding silica gel mold followed by freeze-drying and reduction (Fig. 4a). Among them, GS-fp showed the widest EAB of 37.6 GHz (2.4–40 GHz) and average absorption intensity of −22.9 dB (Fig. 4b). The reason was that the gradient impedance of GS-fp made it easier for EMWs to enter frustum unit cells. The simulation results indicated that EMWs could efficiently enter the interior of GS-fp, and GS-fp has a larger absorption area (Fig. 4c). This work provided an important support for understanding the influence of rGO aerogel macrostructure on EMW absorption performances.

As for microscopic morphology, many studies tried to change the pore structure in GAs to achieve the modulation of EMW absorption properties. According to the former studies, conductive loss derived from induced current will occur when the pore structure is coupled to the incident EMWs [68]. In Fig. 4d, e, Chen *et al.* [69] employed unidirectional freeze casting for fabricating 3D graphene foams with aligned structure (UGF). Inside the aerogel, graphene sheets were assembled almost parallel to form aligned pores. Ultra-high EMW absorption performance with an RL_{min} of −65 dB could be achieved when the coupling of aligned pores and incident EMWs were optimized, which was claimed for the best performance among graphene-based EWAMs. This study provided a convenient and *in-situ* method for tunning the reflection loss and peak frequency by in-plane rotation. Ren's group [70] produced GAs with different microscopic morphologies by introducing ethanol

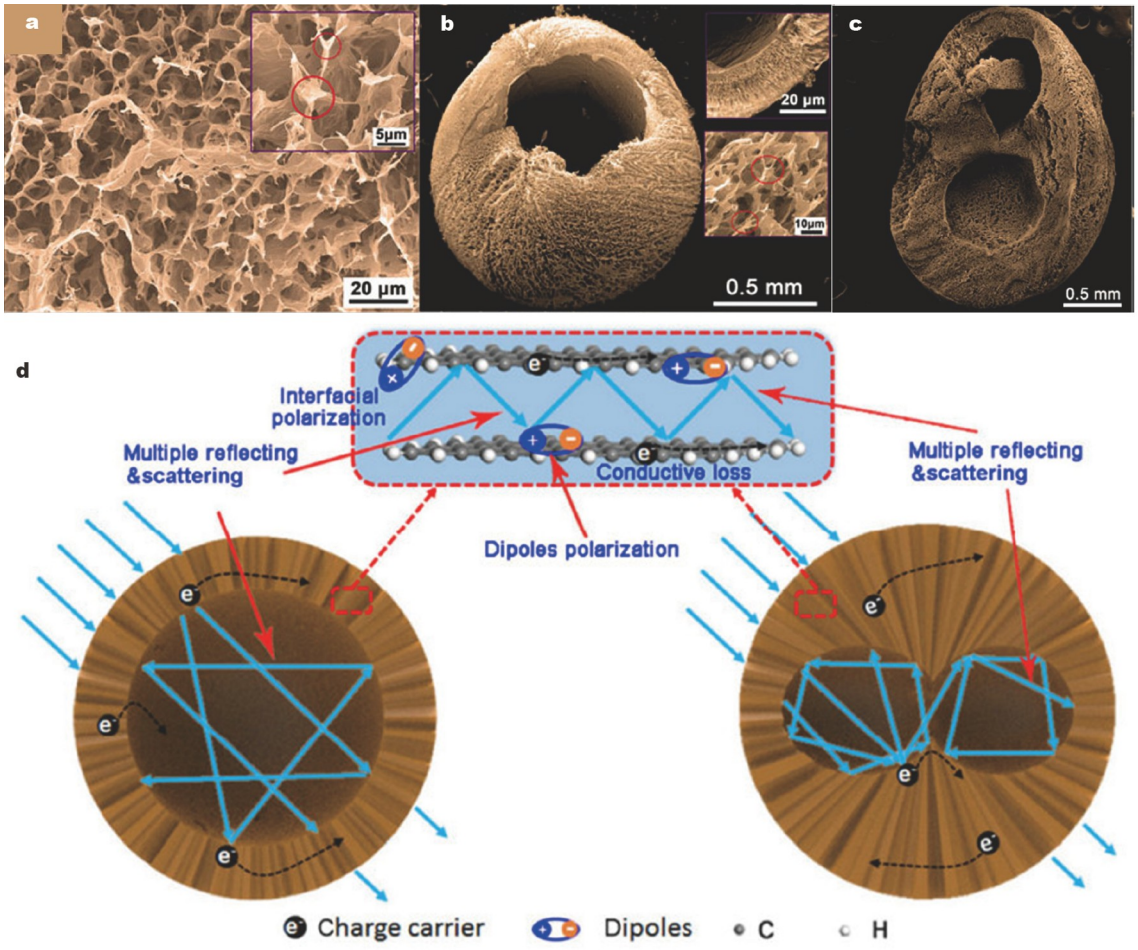

Figure 3 (a) Scanning electron microscopy (SEM) image of the surface morphology of HGAS (the inset is the enlarged image). (b and c) Cross-section morphologies of HGAS and BGAS. The insets in (b) display the thickness of the shell and honeycomb-like structure. (d) The absorption mechanisms of HGAS and BGAS. Reprinted with permission from Ref. [66]. Copyright 2020, Springer.

into the hydrothermal reaction and adjusting the ratio of ethanol to water. Experimental results showed that replacing some of the water with ethanol reduced the surface tension of the solvent, resulting in samples with a fluffier structure and less stacking. Dangling oxygen-containing bonds and exposed defects increased as the agglomeration of graphene decreased, which promoted the polarization effect. Finally, the sample obtained at the ethanol/water ratio of 1:1 achieved a strong RL_{min} of −52.6 dB and a wide EAB of 7.65 GHz. Shao's group [71] reported the preparation of 3D rGO aerogels with tunable pore structures. The manipulation of pore structure was realized through a prereduction strategy. Specifically, the prereduction degree controlled the number of oxygen-containing groups in GO sheets and further influenced the rGO assembly. GO with a low prereduction degree had a large connection gap and loose structure, while rGO with a high prereduction degree would be stacked. Reasonable pore structure could facilitate the formation of 3D conductive networks and the impedance matching. Eventually, the best sample showed a superhigh EMW absorption performance with an RL_{min} of −61.63 dB and a maximum EAB of 7.8 GHz.

3D graphene-based composites

Multivariate composite materials can often make up for the shortcomings of unary materials. For pure 3D graphene materials, problems such as impedance mismatch and poor mechanical properties can be solved by material compositing. The polymer has good mechanical properties and low electrical conductivity, which is considered promising in optimizing the impedance matching and mechanical properties of 3D graphene composites [72,73]. Huang's group [74] introduced polyaramid (PA) into graphene foam. The interfacial π–π interactions were constructed when the PA was coated on graphene skeleton, which led to plentiful interfacial polarization loss (Fig. 5a). Hence, the graphene/polymer composite foam (GF/PA) realized an improved EMW absorption performance with an RL_{min} of −36.5 dB and a wide EAB of 8.4 GHz. PA was a kind of thermostable polymer, and it also served as an antioxidative barrier layer to prevent the oxidation of graphene at high temperatures. Thanks to the protection of PA, the EMW absorption performance of the GF/PA could be completely preserved even after being treated at 300°C in air atmosphere (Fig. 5b). Liao's group [75] developed a kind of thermoplastic polyurethane (TPU)/GA with multi-stage network *via* supercritical CO_2 foaming. The multi-stage TPU/GA network showed a cellular structure, which could improve the reflections and scatterings of the incident EMWs inside the aerogel. The coating of TPU optimized the impedance matching and enhanced the mechanical strength of

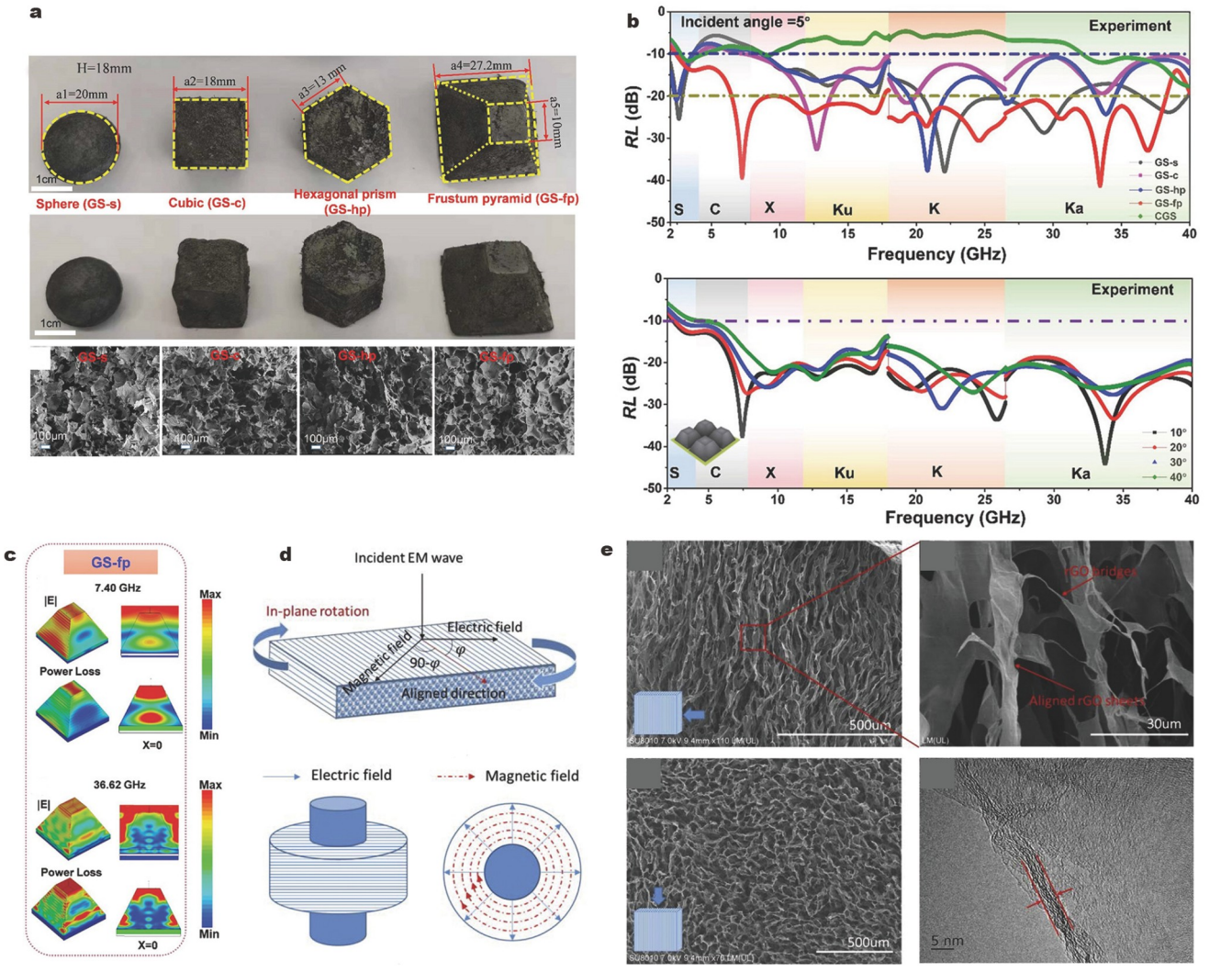

Figure 4 (a) Digital and SEM images of GS-s, GS-c, GS-hp, and GS-fp. (b) The experimental RL of GS with various shapes at 2–40 GHz. (c) Complex electric field intensity time-averaged amplitude distribution and power loss distribution of the GS-hf. Reprinted with permission from Ref. [67]. Copyright 2021, Wiley. (d) Schematic diagram of the coupling angle ϕ between the alignment of the UGF and polarized direction of EMWs, as well as toroidal samples of UGF with alignment transverse to the transmission line. (e) SEM images of the UGF. Reprinted with permission from Ref. [69]. Copyright 2018, Elsevier.

the TPU/GA (Fig. 5c). Inspired by "snowy mountain forest" in nature, Cao and his coworkers [76] designed biomimetic layered EWM shielding/absorbing materials based on graphene, Fe_3O_4 clusters and poly(3,4-ethylenedioxythiophene):poly(4-styrenesulfonate) (PEDOT:PSS) net. Fe_3O_4 clusters were used to adjust impedance matching, while the addition of PEDOT:PSS improved the conductivity drop caused by the loading of Fe_3O_4 clusters. The electromagnetic interference (EMI) shielding performance can be tuned by controlling the amount of graphene and PEDOT:PSS. Finally, this unique biomimetic layered structure has enhanced EMW absorption while achieving good shielding efficiency, which greatly reduces the secondary reflection of EMWs. This unique material is a "green" EMI shielding material and friendly to the external environment.

The combination of graphene with magnetic materials results in enhanced permeability and abundant heterogeneous interfaces [77], which is conducive to the magnetic loss and interfacial polarization loss [78]. In the meanwhile, magnetic materials can also optimize the impedance matching [79], and thus were widely applied in 3D graphene composites [80]. Li's group [81] successfully introduced magnetic particles into GA (Fig. 6a). As shown in Fig. 6b, C@CoFe particles served as fillers to support the stress transferred from the rGO nanosheets. The compressive modulus of C@CoFe/rGO (CCR) composite foam was up to 26 MPa. Simultaneously, with the introduction of C@CoFe particles, the magnetic loss of the composite foam was greatly increased, which brought about better EMW absorption performance. The absorption intensity could reach −46.2 dB at 14.6 GHz and the EAB was up to 13.6 GHz. Wang *et al.* [82] reported the $CoFe_2O_4$ (CFO) nanoparticles embedded N-doped rGO (CFO/N-rGO) aerogel. The embedding of CFO not only adjusted electromagnetic parameters, promoting good impedance matching, but also contributed to the magnetic loss to a certain extent. The CFO/N-rGO composite aerogel (CNGA) exhibited an optimal RL_{min} value of −60.4 dB at 2.1 mm and a broad EAB of 6.48 GHz at 2.2 mm. Wang and Ma [83] fabricated rGO-Fe aerogel (3D rGO/Fe) by a facile hydrothermal method. Fe particles were embedded in rGO sheets (Fig. 6c, d). 3D rGO/Fe shows the RL_{min} and EAB of −34 dB and 6.1 GHz, respectively (Fig. 6e). The improved EMW absorption perfor-

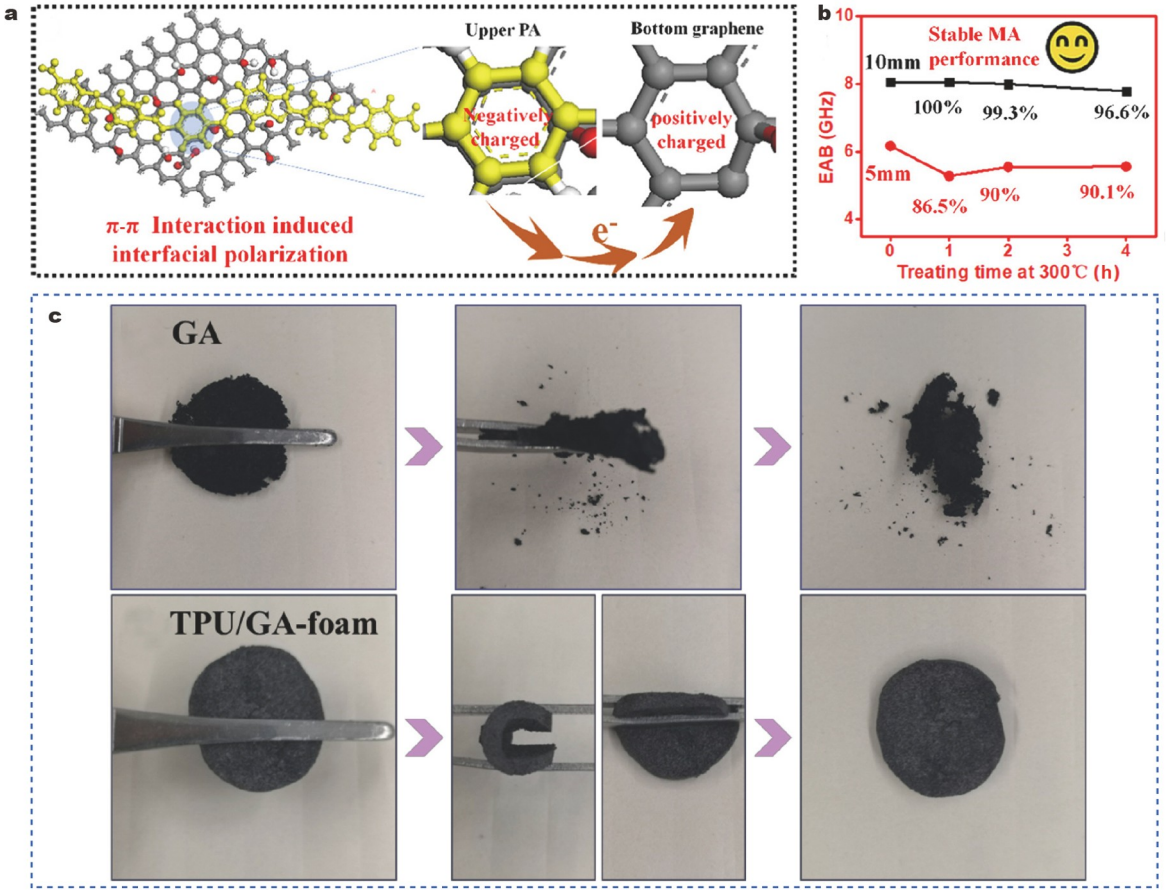

Figure 5 (a) Scheme for π–π interaction-induced interfacial polarization. (b) Retention rate of the EMW absorption performance of PA-coated graphene foam after 300°C heat treatment. Reprinted with permission from Ref. [74]. Copyright 2022, American Chemical Society. (c) Intuitive comparison of mechanical strengths of the GA with and without TPU coating. Reprinted with permission from Ref. [75]. Copyright 2020, Elsevier.

mance could be attributed to four reasons: (1) the combination of carbon materials and magnetic materials optimized the impedance matching and made the EMWs enter absorbers more effectively. (2) Both dielectric loss and magnetic loss contributed to the strong attenuation of EMWs. (3) The embedding of magnetic particles resulted in increasing heterogeneous interfaces, which led to enhanced interfacial polarization. (4) 3D structure tended to cause multiple scatterings of EMWs, which further attenuated the EMW energy. These reasons not only explained the excellent EMW absorption performance of 3D rGO/Fe aerogel, but also summarized the preponderance of the carbon/magnetic composites.

Although the introduction of magnetic materials can improve the EMW absorption performance of EWAMs, the high density and weakened corrosion resistance of the composites become their weakness. Hence, it seems a reasonable solution to combine different types of carbon materials. CNTs are a kind of 1D carbon material that shows promising properties in combination with 3D GAs [84–86]. In Fig. 7a–c, Lv *et al.* [85] achieved ultra-broadband EMW absorption by preparing CNTs/GA composites. The value of RL_{min} at 1.7 mm reached −31.0 dB, and the EAB covered the whole measured frequency range (18–26.5 GHz). Shu *et al.* [86] doped GA with nitrogen and introduced multi-walled CNTs (MWCNTs). The composite had abundant 3D conductive networks, which promoted the conductive loss. Meanwhile, a mass of defects induced by N-doped graphene contributed to the strong dipole polarization. Enhanced conduction loss and polarization loss jointly promoted the improvement of the EMW absorption capacity. The composite foam exhibited an RL_{min} of −69.6 dB and a broad EAB of 4.3 GHz. Besides, some carbides have also attracted attentions. As shown in Fig. 7d, Liu's group [87] reported a $Ti_3C_2T_x$ MXene/rGO composite aerogel anchored with magnetic Ni nanochains (NiMR-H). In previous studies, MXene/GA composites have been considered competitive candidates for preparing broadband EWAMs [88–90]. In this study, magnetic Ni nanochains were introduced into the MXene/rGO composite aerogel to enrich the magnetic loss. Interestingly, by using the finite element simulation and off-axis electron holography technology (Fig. 7g), the authors found that, adjacent Ni nanochains interacted with each other, thereby forming a high-density 3D magnetic-coupling network. The magnetic network made the entire aerogel have strong magnetic loss even in the non-magnetic region. NiMR-H demonstrated an impressive EMW absorption performance with an RL_{min} of −75.2 dB, as well as an EAB of 7.3 GHz at a low filler content of 0.64 wt% (Fig. 7e, f). The authors claimed that it was the best performance among reported MXene-based EWAMs.

Semiconductor materials possess high chemical and thermal stabilities but low EMW absorption capacity, which makes it difficult to serve as EWAMs alone. Thus, the combination of carbon and semiconductor materials became a popular choice

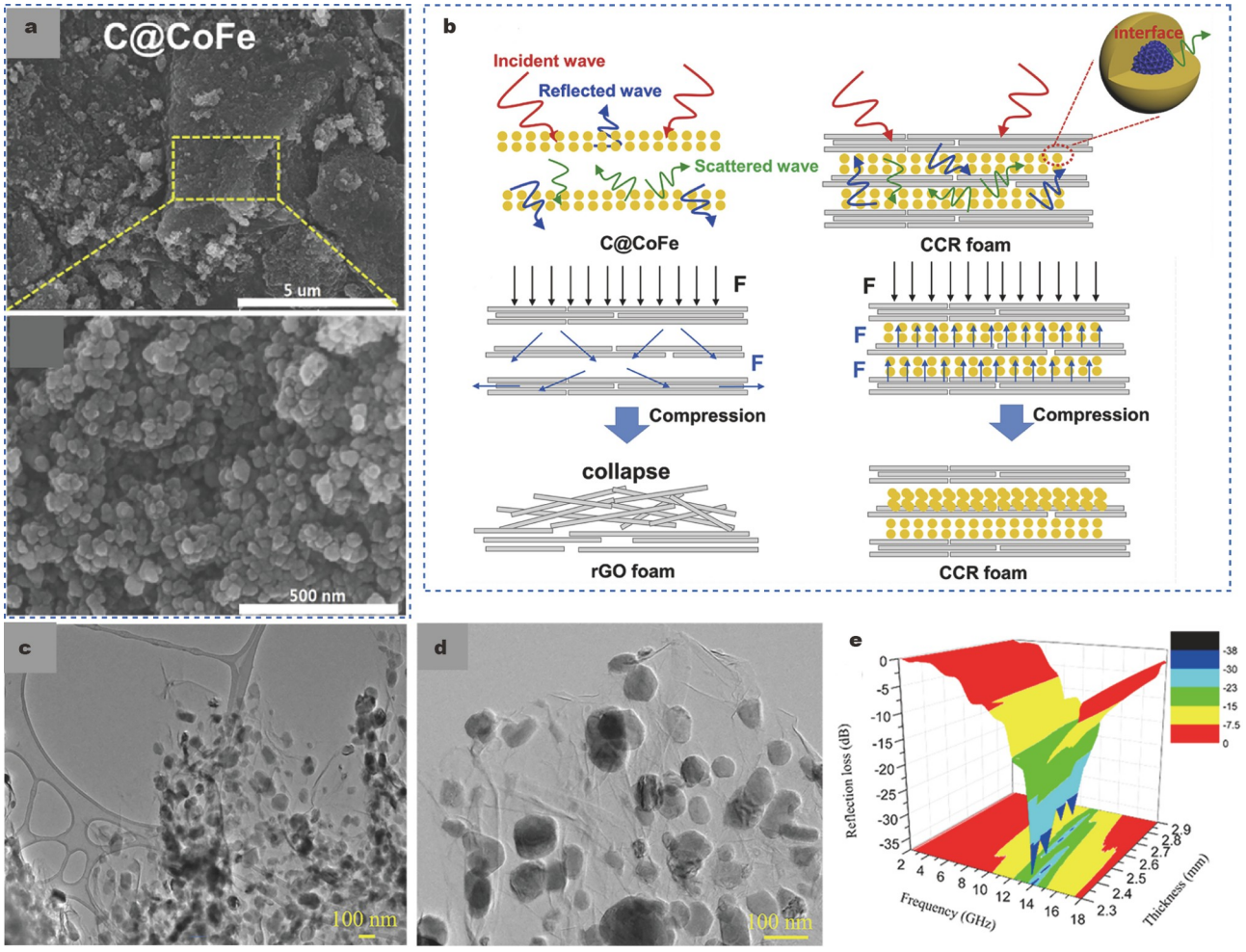

Figure 6 (a) SEM images of the C@CoFe nanoparticles. (b) Diagram of the enhancement of EMW absorption and the reinforcement mechanism of the rGO foam structure. Reprinted with permission from Ref. [81]. Copyright 2020, Elsevier. (c) Transmission electron microscopy (TEM) image and (d) magnified TEM image of the rGO-Fe aerogel. (e) 3D representation of the reflection loss of the rGO-Fe aerogel. Reprinted with permission from Ref. [83]. Copyright 2019, IOP Publishing Ltd.

for researchers. The composite of semiconductor and carbon materials can improve the impedance matching and generate heterogeneous interfaces. Wang and his team [91] grew MoO_3-doped WO_3 nanoflakes on rGO aerogel sheets (rGO-Mo-WO_3). Since MoO_3-doped WO_3 acted as the wave-transparent medium to adjust the complex permittivity, excellent impedance matching could be achieved. EMWs could enter the absorber with minimal reflectivity, greatly improving the EMW attenuation ability of rGO-Mo-WO_3. Meanwhile, jointly with the advantage of 3D structure, rGO-Mo-WO_3 achieved wide EAB of 6.24 GHz and strong absorption of −51.7 dB at a low filler loading of 8 wt%. Besides, the composite of SnO_2 with carbon materials also exhibited impressive performance. Shu's group [92] developed a nitrogen-doped rGO/tin oxide (NrGO/SnO_2) composite aerogel and hold that plenty of tiny SnO_2 particles could form abundant heterogeneous interfaces (Fig. 7h–k), which aroused more interfacial polarization loss. The NrGO/SnO_2 composite aerogel displayed the RL_{min} of −62.3 dB and the EAB of 5.1 GHz at an ultrathin matching thickness (1.6 mm).

Combining multiple materials can balance the properties of composite materials. The outstanding properties of multi-component composites are still attractive. Song's team [93] designed an attapulgite/nickel nanowires/graphene (rGO/ATP/Ni) ternary aerogel. Attapulgite played a role in preventing graphene aggregation and regulating the electromagnetic parameters of ternary composite aerogel, while the nickel nanowires brought on strong magnetic loss. The attapulgite/nickel nanowires/graphene ternary aerogel had an RL_{min} of −47 dB and a wide EAB of 6.8 GHz. Pan's group [94] successfully synthesized delicate "3D helix-2D sheet-1D fiber-0D dot" hierarchical aerogel (GCA-M), combining the 3D helical carbon nanocoils (CNCs), 2D graphene sheets and 1D carbon nanofibers (CNFs) with 0D Fe_3O_4@C core-shell particles. The introduction of CNCs increased the porosity of aerogel and hindered the stacking of graphene, while CNF enriched the electron conduction network. What is more, Fe_3O_4@C not only regulated the dielectric loss, but also offered the magnetic loss. As a result, the hierarchical aerogel showed excellent performance, such that the RL_{min} value was −71.5 dB at 9.5 GHz, and the EAB covered the entire X band.

Biomass-derived 3D materials

Biomass derivatives with abundant sources and various forms are environmentally friendly and renewable. In general, bio-

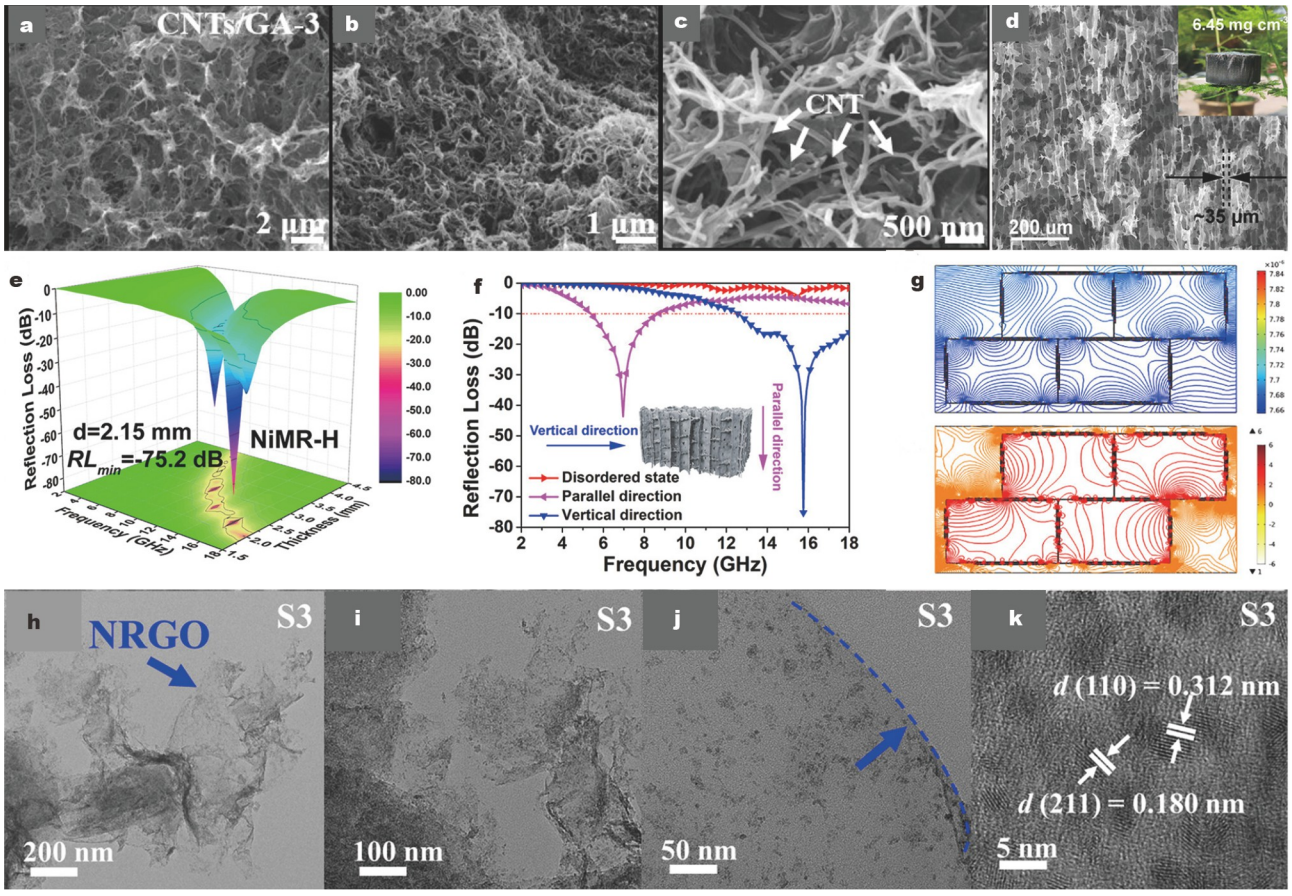

Figure 7 (a–c) SEM images of the CNT/rGO aerogel under different magnifications. Reprinted with permission from Ref. [85]. Copyright 2020, Elsevier. (d) SEM and digital images of the MXene/rGO composite aerogel with Ni nanochains (NiMR-H). (e) 3D reflection loss-frequency curves of the NiMR-H. (f) The EMW absorption performance of the NiMR-H in parallel direction, vertical direction, and disordered state. (g) Finite element simulation for electric-coupling and magnetic-coupling effects of the NiMR-H at 17.02 GHz. Reprinted with permission from Ref. [87]. Copyright 2021, American Chemical Society. (h–k) TEM and high-resolution TEM (HRTEM) images of the nitrogen-doped rGO/SnO_2 composite aerogel. Reprinted with permission from Ref. [92]. Copyright 2021, Elsevier.

mass-based materials originate from wood, plants, and economic crops, such as fruits [95], grains [96] and their wastes [97,98]. Different biomasses have different microstructures, pore distributions and elemental compositions. Notably, some unique structures of biomasses can be preserved, and some elements (such as N, P, and S) can be *in-situ* doped into carbon materials after carbonization, which has key implications on the EMW absorption performance. More importantly, by converting biomasses into carbon materials, some structures that are difficult to achieve by traditional chemical synthesis methods can be obtained, which is the crucial advantage of biomass-derived materials.

Biomass-derived 3D carbon materials

A few biomass-derived materials have suitable electromagnetic parameters, and thus can be directly used as EWAMs. Wu and his coworkers [99] synthesized 3D carbon foam derived from fish skin. The abundant amino acids in fish skin can be used as N and O sources for element doping (Fig. 8a). The doping of N and O induced strong polarization loss, and the 3D structure favored multiple scatterings of incident EMWs. Owing to the uniform doping of N and O as well as the 3D structure with a large specific surface area, the fish skin-derived carbon foam exhibited a favorable EMW absorbing property with an RL_{min} of −52.6 dB and an EAB of 6.3 GHz. Li and his group [100] fabricated the reed-based hierarchical porous carbon. The porous structure effectively improved the impedance matching (Fig. 8b), which allowed the best samples to achieve an outstanding RL_{min} of −63.9 dB and an EAB as wide as 5.4 GHz at 2.0 mm. Ding's group [101] developed 3D carbon foams obtained from wheat straw (Fig. 8e). 3D carbon foam with reasonable microporous structure enabled good impedance matching and multiple reflections for EMWs. In this work, an RL_{min} of −37 dB could be achieved and the EAB was up to 8.8 GHz with only 2.5 mm sample thickness (Fig. 8c, d). Ji's group [102] successfully synthesized the shaddock peel-based carbon aerogel (CA) with interlinked conductive network, which displayed a moderate RL_{min} of −29.50 dB in the X band, and the EAB covered 5.80 GHz at a relatively low thickness of 1.7 mm (Fig. 8f). It was even more remarkable that the shaddock peel-derived CA exhibited good mechanical properties with a maximum compressive stress of 2.435 kPa and excellent thermal insulating property (Fig. 8g). Finally, computer simulation technology (CST) was also applied in this study, which provided radar cross-section (RCS) values for different samples to reflect their practical application prospects (Fig. 8h).

To further improve the EMW absorption performance of pure biomass-derived materials, current modification strategies were

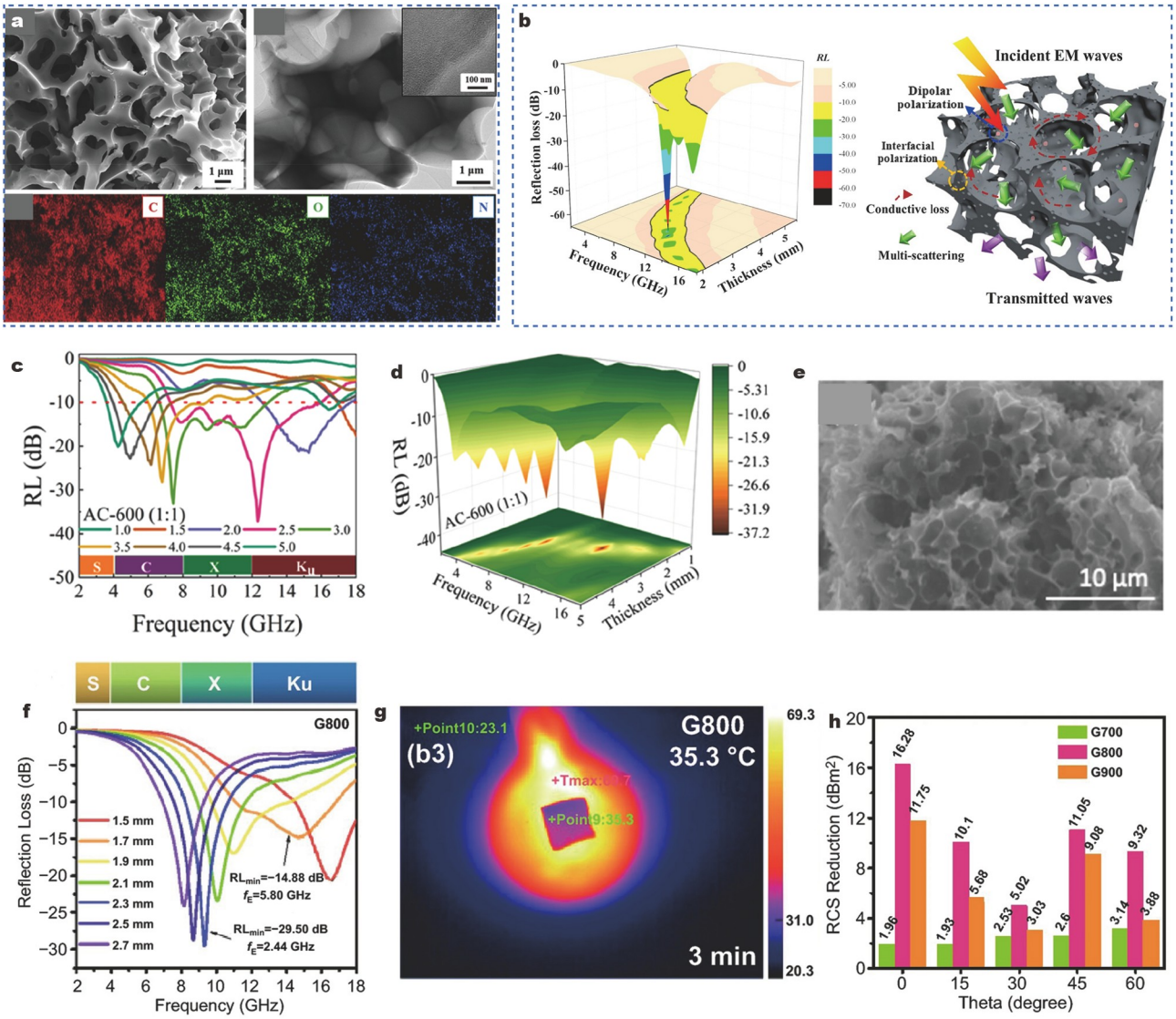

Figure 8 (a) SEM and TEM images of the fish skin-derived carbon foam, as well as corresponding X-ray energy dispersive spectroscopy (EDS) mapping. The inset is the HRTEM of the edge of the carbon foam. Reprinted with permission from Ref. [99]. Copyright 2019, Elsevier. (b) EMW absorption performance and mechanism of reed-derived hierarchical porous carbon. Reprinted with permission from Ref. [100]. Copyright 2021, Elsevier. (c) 3D and (d) 2D reflection loss-frequency curves as well as (e) SEM image of the wheat straw-derived carbon foam. Reprinted with permission from Ref. [101]. Copyright 2021, Elsevier. The (f) reflection loss, (g) thermal insulation and (h) RCS values of the shaddock peel-based CAs. Reprinted with permission from Ref. [102]. Copyright 2021, Springer.

carried out from two aspects, including microstructure modification and element doping. Hence, many studies tuned the pore morphologies by changing the calcination temperature as well as the type and amount of activator. Wu *et al.* [103] prepared rice husk-derived hierarchical porous carbon (BHPC). The microstructure of BHPC was related to the sintering temperature. With the increase of temperature, the pores tended to become larger, and the pore walls were thinner. However, excessive temperature caused pores to collapse, and no pore structure was found on the surfaces of the samples without KOH activation. Therefore, both calcination and activation could change the microscopic morphology of the biochar to a certain extent. As a result, the RL_{min} and EAB of BHPC were up to −47.463 dB and 3.402 GHz, respectively. Similarly, a kind of flower cluster-liked porous carbon, originated from discarded mango seeds, was synthesized by Wang's group [104]. This work also mentioned that the KOH treatment process had a direct effect on the morphology of the final product and further affected the EMW absorption properties of the materials. Porous carbon exhibited a unique flower-like structure with an appropriate amount of KOH, which increased the interfacial polarization to attenuate EMWs. The best sample had excellent EMW absorption performance, and its RL_{min} was up to −68.4 dB, while the EAB covered almost the entire X band. Moreover, RCS was evaluated by computer simulation. The maximum RCS reduction reached 30.4 dB m^2, which was superior to the most of reported studies. Wu's group [105] also focused their research on activators. Pinecone was chosen as raw materials and four different activators (KOH, NaOH, K_2CO_3 and $ZnCl_2$) were used to study the effect of activators on the porous structure. Due to the different activation ability of the four activators, it was found that the amount and type of activators would affect the pore

structure. When the activator was K_2CO_3, a honeycomb-like porous structure was presented, which made a plenty of unconnected cavities. The unconnected cavities made K_2CO_3-treated samples achieve favorable impedance matching and effective multiple reflections. As a result, an RL_{min} of −76.0 dB at 2.1 mm thickness can be achieved.

Some biomass-derived 3D porous carbon materials with novel morphologies have also been discussed recently. Li and his group [106] designed an activated waxberry metamaterial (ACW) for ultra-broadband EMW absorption under low-frequency. Fresh waxberries were pretreated and activated by KOH, which had two purposes: (1) one is to increase the specific surface area by producing plenty of micropores; (2) the other is to increase oxygen-containing functional groups. The final sample formed a unique structure in which the outer layer consisted of hollow tubes, and the inner layer was hollow with porous walls (Fig. 9a). The ACW was assembled into an array for the EMW absorption tests. The RL was less than −10 dB in the frequency range from 1.5 to 40 GHz, which showed incomparable advantages in the low frequency as well as broadband EMW absorption. Silk is one of the most abundant natural protein fiber materials. In Yang's work [107], silkworms-derived carbonized silk fiber mats (SCF) were successful fabricated, which showed an RL_{min} value of −70 dB at 17.6 GHz and 2.5 mm, and the EAB value of 8.7 GHz (9.3–18 GHz) at 3.2 mm thickness (Fig. 9f). By comparison with some former studies, the authors found that absorbers with narrower EAB (<4 GHz) generally had lower loss tangent ($\tan\delta_\varepsilon$) values below 0.4, while a relatively high $\tan\delta_\varepsilon$ range (0.5–0.9) was needed for a wideband absorption performance (EAB > 5 GHz). Nevertheless, severe impedance mismatch occurred when $\tan\delta_\varepsilon$ was greater than 1. In addition, the influence of fiber length on the EMW absorption performance was also investigated. Improved fiber continuity was conducive to higher electrical conductivity. With the increase of the fiber length, the permittivity including both ε' and ε'' increased obviously, which further improved the conductive loss of the SCF.

Element doping provides another way to optimize the EMW absorption performance of biomass-derived carbon materials. Rong *et al.* [108] fabricated natural cotton-derived carbonized fibers (CCFs) with multi-elemental doping. Elements such as C, O, S, P and N, which were naturally present in cotton, could be *in-situ* doped into carbonized cotton by the heat treatment, resulting in significant enhancement and tunability for the EMW absorption performance. In Fig. 9e, the best sample exhibited optimized RL_{min} of −51.94 dB, and the EAB reached 5.5 GHz at the thickness of 1.96 mm. Coincidentally, Liu's group [109] also performed atomic doping on biomass-derived carbon materials to investigate their EMW absorption properties. They developed sulfur-doped hollow carbon microtubes (S-HCMTs) with a network structure. Poplar catkin was used as a carbon precursor, and sulfur powder served as the doping agent. The SEM images of the HCMTs before and after S doping as well as the corresponding EDS spectrum are shown in Fig. 9b–d. S doping is beneficial to conductivity modulation and dipolar relaxation. As a result, the RL_{min} of S-HCMTs can reach −37.4 dB, and the EAB can exceed 8.0 GHz.

Biomass-derived 3D composites

Magnetic materials, semiconductor materials, etc., are often used to modify biomass-derived 3D carbon materials because they can introduce various attenuation mechanisms and modulate the electromagnetic parameters. Recently, there are still a lot of efforts in this direction, which is expected to achieve high-performance EWAMs.

Magnetic materials can effectively improve the impedance matching of composite materials by adjusting the permeability. Liu and his team [110] developed wood-derived BC modified with a series of transition metal alloys. The introduced CoFe not only enhanced the magnetism of composites, but also had a catalytic effect on the graphitization of BC, promoting the potent dielectric loss and magnetic loss as well as optimal impedance matching. Therefore BC/CoFe showed excellent EMW absorption performance with an RL_{min} of −54.4 dB and EAB of 2.4 GHz. Huang's group [111] reported a bark-derived Co-doped porous carbon composite (Co@PC). The sieve tubes in bark formed a special tubular structure, and the introduced Co nanoparticles were distributed on the surfaces of the tubular structure. Owing to the synergy of magnetic loss and dielectric loss, as well as the multiple reflections of incident EMWs, Co@PC exhibited an RL_{min} of −58.4 dB at 8.6 GHz. Utilizing bamboo as the raw material, Bian's group [112] prepared a magnetic biochar for high-performance EMW absorption. When wood and bamboo were chosen to prepare carbon-based materials, the content of lignin may affect the loading of modified substances. As shown in Fig. 10a–h, with the removal of lignin, the porosity between bamboo fiber cells increased, which was easier for iron salts to soak into the bamboo. The authors suggested that delignification is vital in the synthesis process, which directly affects the absorption efficiency of Fe^{3+}/Fe^{2+} and determines the loading of magnetic material as well as the graphitization degree of biochar. With a relatively low lignin content of 7.0%, Fe_3C/biochar composites possessed excellent EMW absorption capacities with an RL_{min} of −45.60 dB and EAB of 5.52 GHz at 1.75 mm. This work explored the delignification process of biomass materials and provided reference for subsequent work. Wu's group [113] prepared Co@Co_3O_4/C materials using fish scales as raw materials (Fig. 10k), which showed a low RL_{min} of −89.3 dB at 2.4 mm and an EAB up to 6 GHz at 2 mm. The authors attributed the excellent performance to the reasonable design of the composite: (1) unique porous structure facilitated impedance matching and conductive loss, and (2) Co@Co_3O_4 provided extra interface polarization and magnetic losses to attenuate the EMWs. Combining the natural cellulose-derived carboxymethylcellulose sodium (CMC-Na) and ZIF-67, An's group [114] fabricated the bimetallic sulfides (Co_xS_y/Ni_xS_y) and magnetic Ni particles embedded N-doped 3D porous carbon (N-Ni-Co_xS_y/Ni_xS_y@C) for EMW absorption. The synergistic effect of ZIF-67 and CMC-Na could optimize the impedance matching of the composite and alleviate the aggregation of magnetic particles. Thanks to the 3D structure and good impedance matching of N-Ni-Co_xS_y/Ni_xS_y@C, an RL_{min} of −48.3 dB and an EAB of 3.95 GHz could be achieved at a thickness of only 1.5 mm. Liu's group [115] fabricated carbonated rGO/Fe_3O_4 (C-rGO/Fe_3O_4) carbon foams with hollow microspheres through the Pickering emulsion gel technology and annealing process. Cellulose nanofibrils and rGO were selected as carbon sources. The obtained samples with hemispherical concave-convex structures could enhance the mechanical properties of carbon foams and lead to multiple reflections of incident EMWs. C-rGO/Fe_3O_4 carbon foams possessed good magnetic properties, compression resilience, and

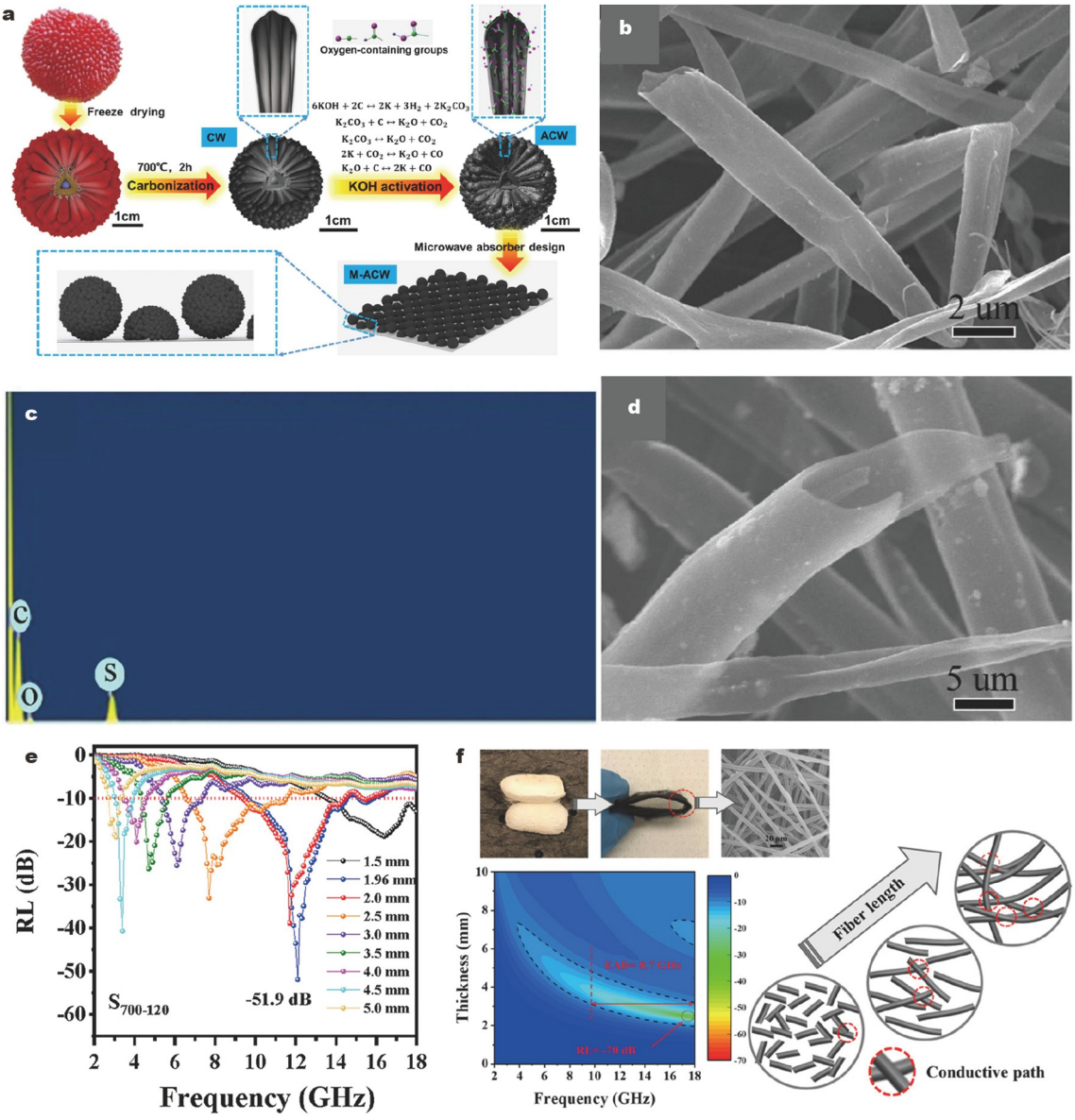

Figure 9 (a) Schematic of the preparation process and microstructure of the ACW. Reprinted with permission from Ref. [106]. Copyright 2021, Elsevier. HCMTs (b) before and (d) after doping S. (c) EDS spectrum of the S-HCMTs. Reprinted with permission from Ref. [109]. Copyright 2021, Springer. (e) EMW absorption performance of the CCFs. Reprinted with permission from Ref. [108]. Copyright 2021, Elsevier. (f) Digital and SEM images of the SCFs, as well as the mechanism of enhanced EMW absorptivity. Reprinted with permission from Ref. [107]. Copyright 2021, American Chemical Society.

fatigue resistance, which showed strong EMW absorption ability with an RL_{min} of −57.50 dB, and a wide EAB of 4.16 GHz. It is worth noting that C-rGO/Fe_3O_4 carbon foams also showed increased conductivity with compression ratio, so it also displayed potential as a wearable sensing material. Zhu's group [116] reported a chitosan-derived ordered porous honeycombed-like CA with embedded Co nanoparticles (Co@C/CG) *via* the directional freeze-casting and subsequent carbonization process. First-principles calculation was applied to illustrate the contributions of conductivity, interfaces, dipoles, and ordered porous structure on EMW absorption. Consequently, the Co@C/CG showed an RL_{min} of −45.02 dB and an EAB of 4.02 GHz. The CST simulation results also verified that the Co@C/CG could attenuate the EMW energy. Besides, the flame retardancy and electrothermal conversion ability of Co@C/CG were also investigated, which meant that the Co@C/CG had a wide application range.

In addition to the studies on the combination of biomass-derived carbon and magnetic materials, some studies have provided new insights into the morphology design and performance factors based on magnetic materials/biochar composites. Helical EWAMs were reported to feature a special chiral structure with adjustable chiral parameters [117,118], which could create the cross-polarization of EMW for advanced EMW absorption [119,120]. However, most of them required complex preparation processes. Zhang and his coworkers [121] discovered a kind of porous chiral material with an elaborate helical structure derived from platanus fruit in nature. Co nanoparticles were introduced through the catalytic self-deposition technology and further induced the growth of CNTs. As a result, the 3D magnetic helical porous carbon fibers (MHPFs) were successfully fabricated (Fig. 10i). The special 3D helical structure of

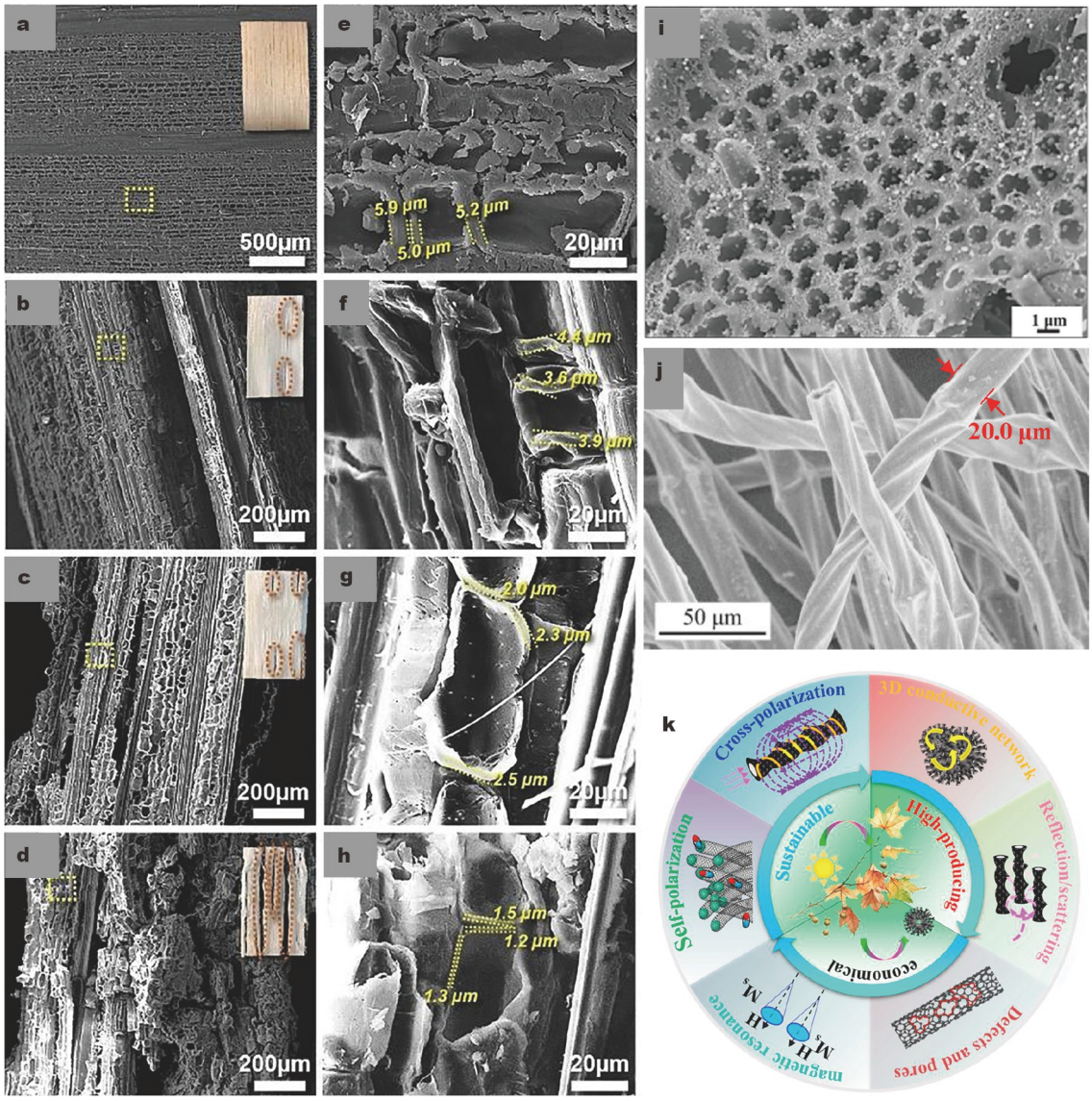

Figure 10 (a–h) SEM images for the bamboo sheets after delignification for 0, 2, 4 and 8 h. Reprinted with permission from Ref. [112]. Copyright 2022, Elsevier. (i) SEM image of the Co@Co_3O_4/C. Reprinted with permission from Ref. [113]. Copyright 2020, Elsevier. (j) SEM image of the 3D MHPFs. (k) Schematic illustration of the possible EMW absorption mechanism and advantages for MHPFs. Reprinted with permission from Ref. [121]. Copyright 2021, Elsevier.

MHPFs could be deemed as an autologous helical coil, being prone to considerable eddy current loss. Benefiting from multiple loss mechanisms and unique structure (Fig. 10j), MHPFs achieved an RL_{min} of −61.08 dB at 2 mm with a low filler loading of 5%. Fang *et al.* [122] reported a medical degreased cotton-derived porous Fe_3O_4/C composite. The authors pointed out that the excessive pore volume made the Fe_3O_4/C transparent to EMWs, while only the moderate porosity facilitated the outstanding EMW absorption performance. Finally, the best sample exhibited an RL_{min} of −22.1 dB and an EAB of 4.4 GHz at a thickness of 2.0 mm. The improvement of composites on absorption performance is often attributed to multiple reasons. It is necessary to clarify the influence of different factors on the final EMW absorption performance, which points the direction for the follow-up design of EWAMs. Li *et al.* [123] chose corncob-derived carbon/Ni (CDC/Ni) composites to study the influences of the graphitization degree, pore size, and surface area on the electromagnetic parameters, impedance matching, attenuation constant, and final EMW absorption performance. The authors indicated that the most important factor affecting the EMW absorption performance was the impedance matching, followed by the electromagnetic loss capability and attenuation constant, and finally the multiple reflections and scatterings of EMWs induced by the 3D structure. In this work, the best sample showed an EMW absorbing performance with −50.25 dB RL_{min} and 2.24 GHz EAB at 1.2 mm.

The combination of biomass-derived 3D carbon materials with 2D and 1D carbon materials can ensure that the composite materials have a low density. 2D, 1D carbon materials, such as highly conductive graphene, and CNTs, are beneficial to forming a network with good conductivity in the 3D framework [124]. Wang *et al.* [125] prepared the CNT/cellulose aerogel (CCA). Due to the excellent heat resistance of lignin, the preparation of BC often requires high temperatures and a long-time carboni-

zation process. Using cellulose as the raw material to produce BC aerogel was a promising method to reduce the carbonization temperature and time. Meanwhile, the introduction of CNTs with high dielectric loss could further reduce the carbonization temperature and processing time of composite aerogels (Fig. 11a). As shown in Fig. 11b, CCA achieved an RL_{min} of −43.6 dB and a wide EAB of 7.42 GHz at 3 mm. Likewise, cellulose was also selected by Liu's group [126]. They developed a cellulose-derived C/rGO aerogel as an EMW absorber with multifunctionalities. Unidirectional cellular structure and GO-enhanced cell walls led to good elasticity and outstanding EMW absorption performance (Fig. 11c). An RL_{min} of −46.11 dB and a maximum EAB of 9.12 GHz could be achieved as exerting 70% compression strain. Remarkably, the C/rGO aerogel also showed effective thermal infrared stealth and heat insulation, exhibiting the adjustable Joule heating performance.

Low conductivity of semiconductors with wide bandgap can improve the impedance matching of composites. The composite of semiconductor materials and biochar has also been investigated. 2D transition metal sulfides possess flaky morphology and good dielectric loss, which are widely used in EWAMs [127,128]. In Zeng's work [129], honeycomb-like NiS_2/SnS_2 nanosheets were successfully grown on popcorn-derived 3D porous carbon (PC-NSS). As a typical dielectric loss-type EWAM, NiS_2 formed the heterogeneous composite with different band gaps together with SnS_2. Therefore, the impedance matching can be modulated, and the interfacial polarization can be improved through combining NiS_2/SnS_2 nanosheets with 3D porous carbon. Owing to the synergistic effect of multiple loss types, PC-NSS displayed an RL_{min} of −52.97 dB at 14.92 GHz and a broad EAB of 4.8 GHz at a matching thickness of 1.57 mm. Zhang *et al.* [130] prepared a stinkhorn-derived porous carbon with self-assembled hollow CuS microflowers (PC@CuS). The addition of CuS introduced abundant interfaces, leading to the strong interfacial polarization under the electromagnetic field of incident EMWs. The synergistic effect of 3D porous carbon with CuS could

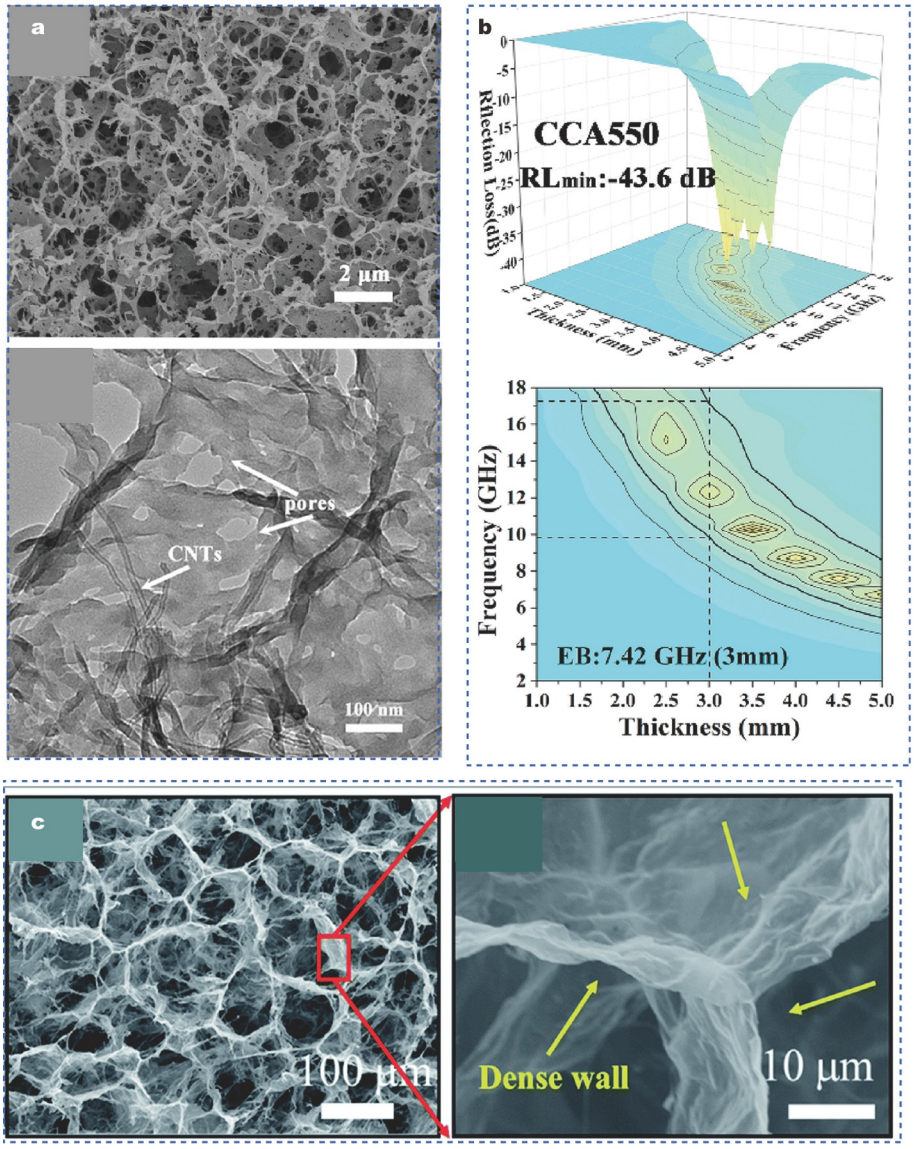

Figure 11 (a) SEM and TEM images of the CNTs/CCA. (b) 3D counter map of the microwave reflection loss of CCA. Reprinted with permission from Ref. [125]. Copyright 2021, Elsevier. (c) SEM images of the C/rGO aerogel. Reprinted with permission from Ref. [126]. Copyright 2021, Royal Society of Chemistry.

achieve satisfactory impedance matching and attenuation capability. Furthermore, fire resistant properties and thermal stealth function were also investigated. PC@CuS not only possessed an EAB of 5.6 GHz and an outstanding RL_{min} of −59.9 dB, but also equipped excellent thermal stealth and flame retardancy. Metal oxide loading is also a common option for BC composites. For example, CeO_2 has low conductivity and high chemical stability, which is suitable for adjusting the electromagnetic parameters of pure carbon materials to achieve the impedance matching. Huang *et al.* [131] successfully synthesized 3D CeO_2/porous carbon for EMW absorption. The transformation from Ce^{4+} to Ce^{3+} could produce oxygen vacancy defects in CeO_2 crystals, which induced potent polarization loss. Combining the advantages brought by 3D structure, the 3D porous CeO_2/carbon achieved an RL_{min} of −56.04 dB at a thickness of 1.9 mm.

Polymer-derived 3D carbon materials

Using polymers as carbon sources to prepare carbon foams is feasible. In the meanwhile, the polymers may be rich in elements such as N, S, O, and F, which can be *in-situ* doped into the carbon materials during the carbonization. Hence, various polymers became popular starting materials for 3D EWAMs.

Melamine foam (MF) was also known as melamine-formaldehyde resin and considered a promising 3D EWAM due to its high porosity (> 99%), accessibility, and N-rich feature. Liu and his coworkers [132] carried out a series of work on MF-based absorbers. A type of MF-derived 3D carbon foam embedded with CuNi alloy nanoparticles (CuNi/CF) was constructed. MF-derived N-rich carbon foam induced the mass of dipole polarization. 3D structure and CuNi alloy nanoparticles caused multiple scatterings of EMWs and strong interfacial polarization. By changing the molar ratio of Cu and Ni, the electromagnetic parameters could be modulated and an RL_{min} of −50.20 dB at 1.6 mm could be achieved. In addition, MoS_2 nanosheets were also loaded onto MF-derived 3D carbon foam (MSCF) [133]. N-rich carbon foam exhibited improved electrical conductivity. The multiple reflections of EMWs could be further enhanced by MoS_2 nanosheets. Consequently, the RL_{min} of MSCF reached −45.88 dB, and the EAB was as wide as 5.68 GHz at 2.2 mm. In addition, MOFs, as a new type of promising EWAMs, possessed abundant pores to realize multiple reflections of EMWs [134–136]. Introducing MOFs into carbon foams is also beneficial to adjusting the impedance matching for efficient EMW absorption. Therefore, ZIF-67 was loaded to MF-derived carbon foam (ZIFCF) by Liu's group [137]. After annealing, ZIF-67 transformed into Co_3O_4 and N-doped carbon anchored on carbon foam (COCF), which could be proved by X-ray diffraction (XRD, Fig. 12a). In Fig. 12b, c, the morphologies of samples could be well maintained after annealing. The ZIF67-derived Co_3O_4 adjusted the electromagnetic parameters and enhanced the magnetic loss. Unique 3D structure of the COCF contributed to the scatterings of EMWs and the movement of carriers (Fig. 12d). Finally, the best sample had an RL_{min} of −46.58 dB and an EAB of 5.4 GHz. Zhao and his coworkers [138] found that under the catalysis of Co nanoparticles, 1D CNTs would grow on the surface of the MF-derived 3D carbon foam (Co/CMF). The authors proposed that CNT whiskers enhanced the electrical conductivity (3.7×10^{-2} S m^{-1}), the

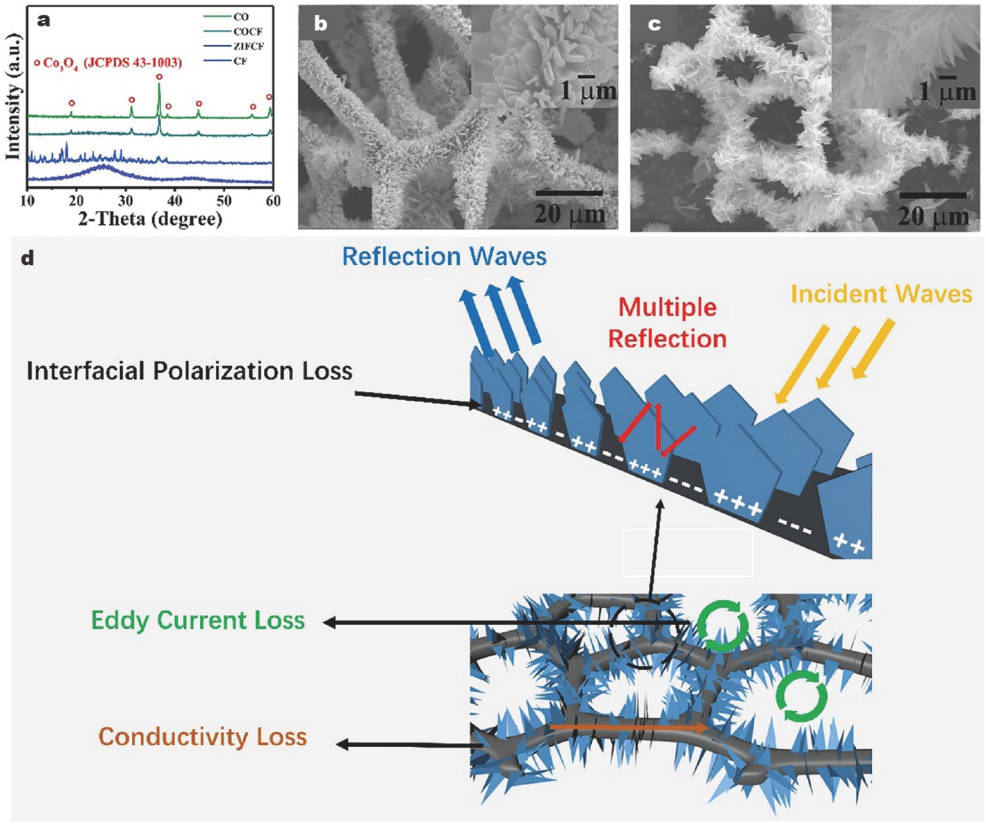

Figure 12 (a) XRD of ZIF-67-loaded carbon foam before (ZIFCF) and after (COCF) annealing. SEM images of the (b) ZIFCF and (c) COCF (the insets exhibit the magnified SEM images). (d) Schematic of the EMW adsorption mechanisms for COCF. Reprinted with permission from Ref. [137]. Copyright 2021, Elsevier.

thermo-oxidative stability, and elasticity of the composite. Hierarchical structures formed abundant conductive networks, and Co nanoparticles enhanced the magnetic loss. As a result, the Co/CMF showed an RL_{min} value of −46.2 at 2.0 mm, the corresponding EAB was 3.9 GHz. Ceramic materials such as SiC are considered to have potential as EWAMs. Li *et al.* [139] fabricated SiC/MF-derived carbon foam composites (S_{nw}SCF) by chemical vapor deposition (CVD) and chemical vapor infiltration (CVI) processes. Carbon foam, SiC coating, and SiC nanowires formed the hierarchical 3D structure, which was favorable for EMW absorption. The optimal RL_{min} and EAB of S_{nw}SCF reached −31.216 dB and 4.1 GHz at 1.5 mm. Zhao *et al.* [140] loaded Fe_3O_4 magnetic nanoparticles on melamine-formaldehyde resin and then carbonized the composite to obtain magnetic graphite-like C_3N_4/carbon foam (MCMF). The magnetic particles (α-Fe, Fe_3C or Fe_3O_4) increased the magnetic loss of the material to a certain extent. More importantly, graphite-like C_3N_4 enriched the interfacial polarization and optimized the impedance matching, making the sample achieve an RL_{min} of −47.38 dB at 3.90 mm.

Apart from melamine-formaldehyde resin, other resins also have potentials as 3D carbon precursors. Li and his group [141] reported a phenolic foam-derived magnetic carbon foam (MCF), which showed a solid 3D foam architecture with interconnected cells and decorated magnetic particles such as α-Fe, Fe_2O_3 and Fe_3C (Fig. 13a, b). By changing the foaming process, the samples had different cell-wall thicknesses. The authors found that the conductivity of samples increased with the cell-wall thickness, which would further affect the EMW absorption behavior of the MCFs. Through controlling the thickness of cell walls, the MCF achieved an RL_{min} of −54.02 dB at 3.05 mm (Fig. 13c).

Some 3D carbon materials can also be obtained through the polymerization and carbonization of organic components. Liu *et al.* [142] developed a N-doped porous CA (NPCA) by a gelatin process of rigid organic polymer aerogel and a subsequent pyrolysis process. As the heat treatment temperature rose, N heteroatoms declined and electron vacancies increased, which resulted in the weakening of dipole polarization and the enhancement of interface polarization. Based on the electron density distribution obtained by first-principles calculations for each sample, it is found that the content of N heteroatoms and vacancies needs to be balanced to achieve the strong loss ability. Eventually, *via* an appropriate heat treatment, the RL_{min} and EAB of NPCA were up to −61.7 dB and 5.3 GHz, respectively. Similarly, Yang's group [143] developed ferrite/CA composites (Fe_3O_4/CA) by vacuum impregnation as well as the coprecipitation of iron ions. Utilizing sol-gel polycondensation of 1,3-dihydroxybenzene and formaldehyde, the CAs with low density and abundant pores were obtained. Ferrite was used as a regulator for the impedance matching. Eventually, the Fe_3O_4/CA exhibited an RL_{min} of −57.0 dB at 5.3 mm and a broad EAB of 5.3 GHz at 1.8 mm.

Zhang's group [144] reported a magnetic metal-implanted hierarchical porous carbon network (HPC/M), which was derived from poly(vinylpyrrolidone) (PVP) through the freezing-drying and carbonization processes. Water-soluble sodium chloride (NaCl) served as a soft template to form hierarchical porous structure. The existence of abundant oxygen-containing functional groups and defects in porous carbon brought about intensive dipole polarization. Magnetic Ni or Co not only enhanced the magnetic loss of the material but also promoted the dielectric loss of the material by catalyzing the graphitization of carbon. Finally, an excellent absorption with the RL_{min} of −58.7 dB at 2.9 mm was realized.

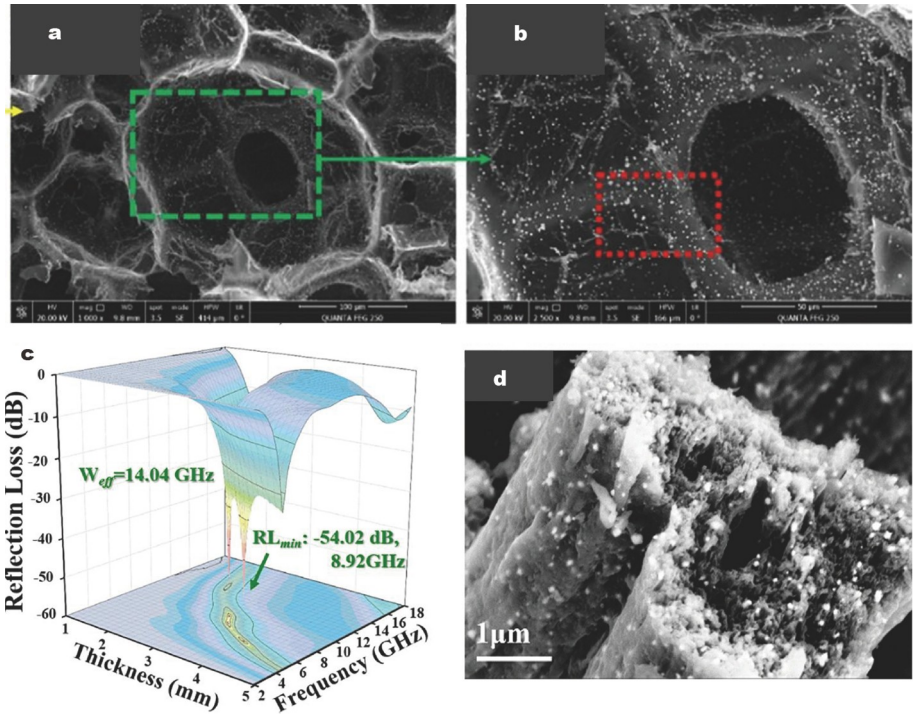

Figure 13 (a, b) SEM images of the cross-section of phenolic foam-derived MCF with different magnifications. (c) 3D RL_{min} values of phenolic foam-derived MCF. Reprinted with permission from Ref. [141]. Copyright 2020, Elsevier. (d) SEM image of the Fe_3O_4/Fe_3C-supported porous carbon. Reprinted with permission from Ref. [145]. Copyright 2021, Springer.

The preparation of 3D carbon fiber networks by electrospinning and calcination is a more convenient and controllable technique compared with the template method. Li's group [145] synthesized porous magnetic absorbers *via* carbonizing $Fe(acac)_3$/polyacrylonitrile (PAN) composite fiber. After carbonization, the $Fe(acac)_3$/PAN composites obtained by electrospinning were transformed into Fe_3O_4/Fe_3C-supported porous carbon. This preparation process allowed magnetic particles to exist on the surface and in the inner of the fibers (Fig. 13d), preventing the agglomeration of particles and the blocking of pores. At the carbonization temperature of 1000°C, The Fe_3O_4/Fe_3C-supported porous carbon obtained good magnetic loss capability, achieving an RL_{min} of −29.27 dB at 1.5 mm. Coincidentally, Wang *et al.* [146] successfully synthesized a porous 3D hierarchical structure through electrospinning and carbonization. PAN and PVP were chosen as raw materials for preparing CNFs, and $Co_{0.2}Fe_{2.8}O_4$ magnetic particles were introduced to enhance the magnetic loss of the composites. As a result, this sample achieved an RL_{min} of −43.45 dB and an EAB of 5.85 GHz. Qiao *et al.* [147] fabricated a kind of PVP-derived carbon fibers by electrospinning and carbonization. MnS nanoparticles were embedded into fibrous carbon to restrain the permittivity of carbon fibers, achieving improved impedance matching. As a result, the MnS/C nanocomposite fibers possessed strong EMW absorbing ability with an RL_{min} of −68.9 dB at 3.6 mm and an EAB of 7.2 GHz at 3.3 mm. Meanwhile, magnetic Co nanoparticles and MnO nanoparticles were also proposed to fabricate C/Mn/Co nanocomposite fibers [148]. Co nanoparticles could bring about magnetic loss, while MnO could serve as an impedance modulator. Finally, thanks to multiple loss mechanisms, rich heterogeneous interfaces, and multiple reflections, C/Mn/Co nanocomposite fibers achieved an EAB of 6.3 GHz, and an RL_{min} of −71.7 dB at 14.1 GHz and 2.6 mm.

Other 3D carbon materials

CNTs have attracted extensive attention from academia, due to their low density and high conductivity [149–151]. Recently, reports on preparation of 3D CNT foams and arrays also emerged [152–154]. Zhao's group [152] developed 3D CNT foams by the resorcinol-formaldehyde resin template method. Subsequently, CNT foam/epoxy composites were obtained by the vacuum impregnation method. The highly porous structure alleviated the impedance mismatch, and the resin substrate with low dielectric loss made it easier for EMWs to enter the material. Finally, CNT foam/epoxy composites had an excellent RL_{min} of −42.13 dB. Zhu and her coworkers [154] fabricated CoNi particles-encapsulated N-doped CNT arrays (CoNi@NCNTSs) with 3D architecture. CNT arrays provided lots of pores and interfaces, and the magnetic transition-metal particles induced eddy current loss. Moreover, defects, and N dopants led to dielectric relaxation loss, and consequently an RL_{min} of −49.82 dB was presented.

Some commercial 3D carbon materials such as carbon fiber felt and carbon cloth usually originated from PAN, have also been studied. These commercial materials are not only readily available but also suitable for large-scale production. These 3D carbon materials possessed interconnected conductive network and plentiful pores, which was in favor of EMW absorption. Dong's group [155] prepared a carbon fiber felt with hydrothermal carbon (HC) and silicon-boron carbonitride (SiBCN) coating (HC-CF/SiBCN). HC coating protected the carbon fiber felt at low temperatures, while SiBCN, as a high-temperature-resistant component, ensured the oxidation resistance of the material above 1000°C. Tunability of effective EMW absorption was achieved by adjusting the thickness of HC coating. With the synergistic effect of HC and SiBCN, the impedance matching of HC-CF/SiBCN could be optimized and the RL_{min} was up to −52.08 dB at 1.8 mm. Meanwhile, the authors also fabricated SiOC/CFs by a precursor infiltration and pyrolysis processes. Methyltrimethoxysilane (MTMS) and dimethyldimethoxysilane (DMDMS) were selected as raw precursors [156]. The presence of SiOC ceramics greatly improved the high temperature oxidation resistance and mechanical stability of SiOC/CFs composites. As for EMW absorption, RL_{min} was up to −62.9 dB at 2.72 mm. Shui and his group [157] also synthesized SiOC and SiC nanowires-loaded carbon fiber felts (SiOC/SiCnws/CFs) composites, which illustrated excellent mechanical and EMW absorption properties of ceramic-loaded carbon fiber felt. The RL_{min} and EAB of SiOC/SiCnws/CFs reached −48.2 dB and 3.06 GHz at 3.6 mm, respectively.

Based on the flexible and conductive characteristics, carbon cloth is suitable for the starting material of EWAMs. Liu *et al.* [158] selected pre-treated carbon cloth as the substrate and loaded Co-MOF precursor on it. Subsequently, carbon cloths modified with N-doped porous carbon nanoplates and CoS_2 (CC@NPC/CoS_2) were obtained after the carbonization and sulphuration processes. The hierarchical morphology is shown in Fig. 14a–c. Carbon cloth could serve as an electron transport channel to ensure the conductivity of the composite, porous carbon could increase the refractions and reflections of EMWs, while embedded Co_2S particles could effectively adjust the impedance matching. Under this synergistic effect, CC@NPC/CoS_2 realized an RL_{min} of −59.6 dB and a wide EAB of 7.2 GHz (Fig. 14d, e). Yin *et al.* [159] built an absorbing model based on 3D woven fabrics (3DWF) for finite element analysis. CST simulation demonstrated that the EAB increased with increasing thickness of 3D woven fabrics. In addition, smaller yarn cross section ellipse and larger fiber volume fraction led to better EMW absorption performance. In this study, a good match between theoretical and experimental values was shown in the frequency range of 1–15 GHz, which provided an important theoretical guidance for designing carbon fiber fabrics such as carbon cloth.

COMPARISON OF 3D CARBON MTERIALS

Here, we summarized the preparation processes and modification strategies of various carbon materials (Fig. 15). The properties of the above-mentioned representative materials were summarized in Tables 1–4 for comparison, respectively.

To sum up, among all kinds of 3D carbon materials, 3D graphene-based materials show lower filler loading, stronger RL_{min} and wider EAB overall. This can be attributed to the low density and high conductivity of graphene. Nevertheless, poor mechanical properties of 3D graphene render a vulnerable structure. High cost is also a major constraint on commercial application of graphene-based materials.

As for biomass-derived 3D carbon materials, they have incomparable advantages over other materials in terms of economy, environmental friendliness, and easy availability. Traditional biomass materials such as wood, peels, and seeds seem to require a larger filler loading, which may be attributed to the relatively high density. In sharp contrast, emerging biomass-

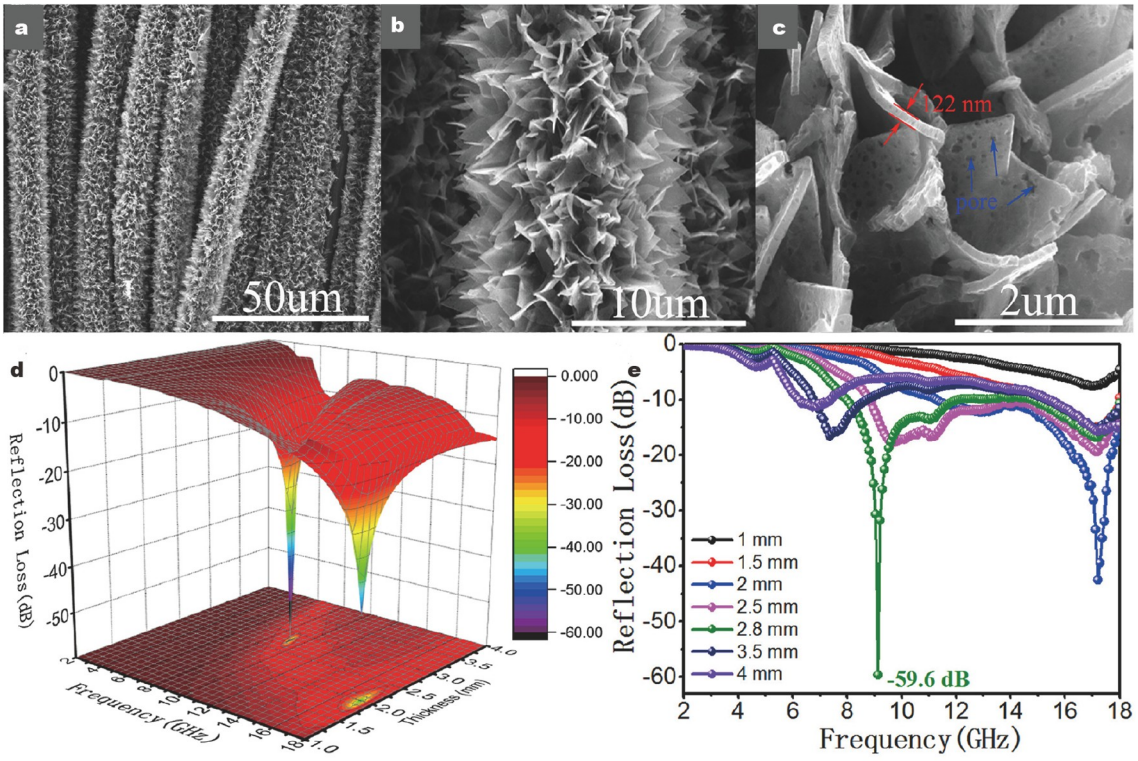

Figure 14 (a–c) SEM images of the CC@NPC/CoS_2 at different magnifications. (d) 3D and (e) 2D RL_{min} values of the CC@NPC/CoS_2. Reprinted with permission from Ref. [158]. Copyright 2020, Elsevier.

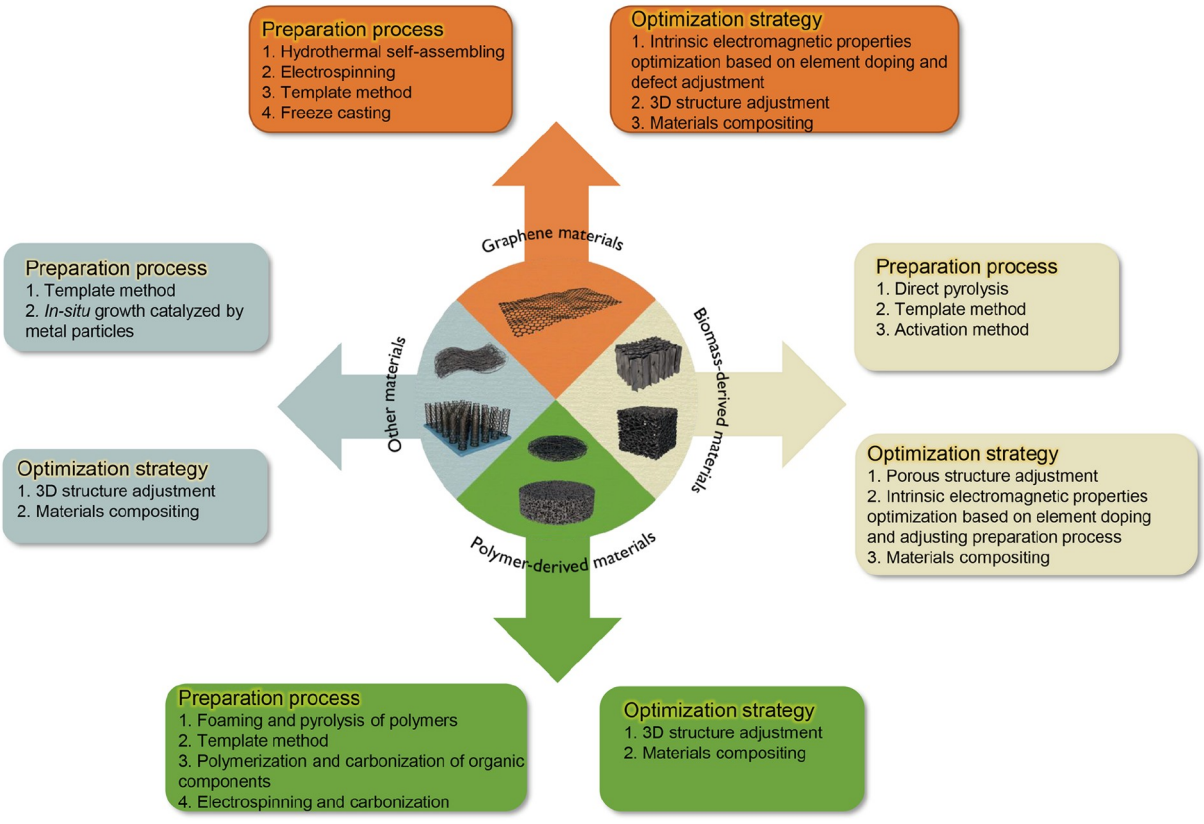

Figure 15 Preparation processes and optimization strategies of various carbon materials.

Table 1 EMW absorption performances of 3D graphene-based materials

Absorber	RL_{min} (dB)	EAB (GHz)	Thickness (mm)	Filler loading (wt%)	Ref
NGF	−53.9	4.56	3.5	5	[64]
rGO aerogel with I^+ modulation	−52.8	6.8	2.5	2	[65]
GA spheres with hollow structures	−52.7	–	2.3	5	[66]
rGO aerogels with tunable pore structures	−61.63	7.75	3.3	0.74	[70]
Graphene/PA foam	−34.2	6.14	5.0	–	[74]
C@CoFe/rGO composite foam	−46.2	–	2.53	50	[81]
$CoFe_2O_4$ nanoparticles-embedded N-doped rGO	−60.4	5.92	2.1	20	[82]
rGO-Fe aerogel	−34.0	6.1	2.7	10	[83]
Nitrogen-doped rGO/MWCNTs composite aerogel	−46.3	–	1.9	15	[84]
CNTs/GA	−31.0	8.5	1.7	4	[85]
3D nitrogen-doped rGO/MWCNT composite foams	−69.6	4.3	1.8	8	[86]
MXene/rGO composite aerogel with Ni nanochains	−75.2	5.4	2.15	0.64	[87]
MoO_3-doped WO_3 nanoflakes decorated rGO aerogels	−51.7	6.24	2.95	8	[91]
Nitrogen-doped rGO/SnO_2 composite aerogel	−62.3	–	3.5	30	[92]
Attapulgite/nickel nanowires/graphene	−47.0	5.74	2.0	–	[93]
“3D-2D-1D-0D” hierarchical aerogels	−55.1	5.0	1.9	15	[94]

Table 2 EMW absorption performances of biomass-derived materials

Absorber	RL_{min} (dB)	EAB (GHz)	Thickness (mm)	Filler loading (wt%)	Ref
Fish skin-derived carbon foam	−52.6	6.3	2.6	30	[99]
Reed-derived porous carbon	−63.9	5.4	2.85	10	[100]
Wheat straw-derived carbon foam	−37.0	8.8	2.5	10	[101]
Shaddock peel-based CA	−29.50	5.80	1.7	20	[102]
BHPC	−47.46	3.402	2.8	10	[103]
Mango seed-derived porous carbon	−68.4	–	2.2	20	[104]
Pinecone-derived porous carbon	−76.00	–	2.1	16.67	[105]
Carbonized silk fiber mats	−70.0	–	2.5	5	[107]
CCFs	−51.94	5.5	1.96	33	[108]
S-HCMTs networks	−37.4	–	6.0	35	[109]
BC/CoFe	−54.4	2.6	2.4	10	[110]
Co-doped porous carbon composite	−58.4	–	3.22	30	[111]
Fe_3C/biochar	−45.60	5.5	4.24	30	[112]
Co@Co_3O_4/C	−89.3	4.56	2.4	16.7	[113]
N-Ni-Co_xS_y/Ni_xS_y@C	−48.3	3.95	1.5	25	[114]
Carbonated rGO/Fe_3O_4	−57.5	4.16	2.0	–	[115]
Ordered porous CA with Co nanoparticles	−45.02	4.02	1.5	30	[116]
MHPFs	−61.08	2.1	2.0	5	[121]
Cotton-derived porous Fe_3O_4/C composite	−22.1	4.4	2.0	50	[122]
CDC/Ni composite	−50.25	2.24	1.2	33.3	[123]
CNTs/CCA	−43.6	7.42	3.0	7	[125]
Cellulose-derived C/rGO aerogel	−46.11	9.12	2.7	0.8	[126]
NiS_2/SnS_2-loaded porous carbon	−52.97	4.8	1.57	25	[129]
Porous carbon@CuS	−59.9	5.6	1.76	15	[130]
CeO_2/porous carbon	−56.04	–	1.9	20	[131]

derived carbon materials such as cellulose and silk fibers show significantly lower filler loading, which may become a new trend [160]. However, the microscopic morphology, which depends on the original structure of biomass, is difficult to be customized, making it hard to find the optimal structure for EMW absorption. Furthermore, widely sourced biochar makes the performance consistency of the final product an issue worth considering.

For polymer-derived materials and other materials, some commercial materials, such as MF, carbon cloth, carbon felt, on

Table 3 EMW absorption performances of polymer-derived materials

Absorber	RL_{min} (dB)	EAB (GHz)	Thickness (mm)	Filler loading (wt%)	Ref
CuNi/carbon foam	−50.2	–	1.6	40	[132]
MoS_2-loaded carbon foam	−45.88	5.62	2.2	40	[133]
Co_3O_4-anchored carbon foam	−46.58	5.4	3.3	40	[137]
Co/carbon foam	−46.2	3.9	2.0	–	[138]
SiC/carbon foam	−31.216	4.1	1.5	50	[139]
Magnetic graphite-like C_3N_4/carbon foam	−47.38	–	3.9	15	[140]
Phenolic foam-derived MCFs	−54.02	–	3.05	15	[141]
NPCA	−61.7	5.3	2.6	20	[142]
Fe_3O_4/CA	−57.0	–	5.3	10	[143]
Hierarchical porous carbon/Ni	−58.7	–	2.9	20	[144]
Fe_3O_4/Fe_3C-supported porous carbon	−29.27	–	1.5	15	[145]
3D hierarchical carbon with $Co_{0.2}Fe_{2.8}O_4$ particles	−43.45	5.85	3.0	50	[146]
MnS/C nanocomposite fibers	−68.9	–	3.6	30	[147]
C/Mn/Co nanocomposite fibers	−71.7	–	2.6	15	[148]

Table 4 EMW absorption performances of other 3D carbon materials

Absorber	RL_{min} (dB)	EAB (GHz)	Thickness (mm)	Filler loading (wt%)	Ref
3D CNT foam/epoxy composites	−42.13	1.6	2.9	–	[152]
CoNi@N-doped CNT arrays	−49.82	–	3.5	20	[154]
Carbon fiber felt/SiBCN	−52.08	–	1.8	30	[155]
SiOC/carbon fiber felt	−62.9	–	2.72	30	[156]
SiOC and SiC nanowires/carbon fiber felts	−48.2	3.06	3.6	50	[157]
Carbon cloth@N-doped porous carbon/CoS_2	−59.6	7.2	2.8	30	[158]

the one hand, are readily available and have the potential for large-scale application. On the other hand, their structures can hardly be further adjusted. In addition, commercial carbon cloth and carbon felt tend to have relatively high density and high graphitization degree, so they are at a disadvantage in terms of filler loading. Simultaneously, the optimization of impedance matching needs to be seriously considered.

CONCLUSION

In this review, we summarized the research of 3D porous carbon-based EWAMs in the past three or four years. These EWAMs were divided into four categories according to raw materials: graphene materials, biomass-derived materials, polymer-derived materials, and other materials. Among them, some studies reported excellent EMW absorption performance, and some studies presented instructive conclusions, which are all beneficial to promoting the development of 3D porous carbon-based EWAMs.

We found that some recent studies are developing towards multi-functionalities and practicality. The development of multi-functionalities may find new application directions for these materials, making them continue to shine in the field of cross-research. For example, some materials have explored the possibility of being used as sensing materials or wearable materials. In the meanwhile, the flame retardancy, cold resistance, high-temperature stability, mechanical strength, and compressibility of EWAMs have also attracted more and more attention, which shows that the academia is considering the application of the EWAMs in more demanding scenarios. Moreover, we also found that researchers turn their attention from traditional biomass materials (such as wood and grain) to emerging biomass materials such as cellulose and silk, which means that both raw materials and preparation processes will be more low-carbon, sustainable and environmentally friendly. This is undoubtedly a desirable change. It is also worth noting that computer techniques such as first-principles calculations and finite element simulations are also increasingly appearing in recent research. This indicates that researchers have begun to understand the effect of materials on EMW absorption at the molecular or atomic scale, and to predict the possibility of materials in practical applications. The introduction of computer technologies provides advance guidance for the selection and design of materials and makes predictions about the actual performance in different application scenarios, which greatly reduces the blindness of material synthesis and enhances the possibility of practical applications.

At the same time, we should also realize that the current research still has some shortcomings. (1) Most of the studies are still stuck in the preparation of materials, the adjustment of process, and the regulation of morphology. However, the EMW absorption theory needs to be developed urgently. Few of the current studies can provide general conclusions and universal recommendations. (2) Although composite materials alleviate the problems of poor impedance matching, it is sometimes difficult to clarify the respective roles of different components. Meanwhile, composite materials also bring about the high density and poor corrosion resistance. (3) Among the studies summarized, few of materials were claimed to be mass-produced. Truly marketable materials need to be further developed.

In the end, 3D porous carbon-based EWAMs have promising

prospects and deserve our unremitting efforts. Many of the results summarized here provide a good starting point for further studies and trials, but also that there is a lot of room for the improvement of 3D porous carbon-based EWAMs. In our opinion, on the premise of ensuring the EMW absorption performance, it is a bright road to consider more practical indicators and explore new application scenarios. Plus, utilizing computer technology to develop EMW absorption mechanisms and screen materials is also of far-reaching significance. We expect this review to enable the research community to be inspired by multitudinous 3D porous carbon-based EWAMs, thereby promoting the advancement of the entire research field.

Received 27 April 2022; accepted 9 June 2022; published online 8 September 2022

1 Cai Z, Su L, Wang H, *et al.* Alternating multilayered Si_3N_4/SiC aerogels for broadband and high-temperature electromagnetic wave absorption up to 1000°C. ACS Appl Mater Interfaces, 2021, 13: 16704–16712
2 Marra F, Lecini J, Tamburrano A, *et al.* Electromagnetic wave absorption and structural properties of wide-band absorber made of graphene-printed glass-fibre composite. Sci Rep, 2018, 8: 12029
3 Qiao J, Zhang X, Liu C, *et al.* Non-magnetic bimetallic MOF-derived porous carbon-wrapped TiO_2/$ZrTiO_4$ composites for efficient electromagnetic wave absorption. Nano-Micro Lett, 2021, 13: 75
4 Yang W, Zhang Y, Qiao G, *et al.* Tunable magnetic and microwave absorption properties of $Sm_{1.5}Y_{0.5}Fe_{17-x}Si_x$ and their composites. Acta Mater, 2018, 145: 331–336
5 Qiao J, Zhang X, Xu D, *et al.* Design and synthesis of TiO_2/Co/carbon nanofibers with tunable and efficient electromagnetic absorption. Chem Eng J, 2020, 380: 122591
6 Zhang X, Jia Z, Zhang F, *et al.* MOF-derived $NiFe_2S_4$/porous carbon composites as electromagnetic wave absorber. J Colloid Interface Sci, 2022, 610: 610–620
7 Zhang M, Cao MS, Shu JC, *et al.* Electromagnetic absorber converting radiation for multifunction. Mater Sci Eng-R-Rep, 2021, 145: 100627
8 Cao MS, Wang XX, Zhang M, *et al.* Electromagnetic response and energy conversion for functions and devices in low-dimensional materials. Adv Funct Mater, 2019, 29: 1807398
9 Zeng Z, Jiang F, Yue Y, *et al.* Flexible and ultrathin waterproof cellular membranes based on high-conjunction metal-wrapped polymer nanofibers for electromagnetic interference shielding. Adv Mater, 2020, 32: 1908496
10 Balci O, Polat EO, Kakenov N, *et al.* Graphene-enabled electrically switchable radar-absorbing surfaces. Nat Commun, 2015, 6: 6628
11 Han C, Zhang M, Cao WQ, *et al.* Electrospinning and *in-situ* hierarchical thermal treatment to tailor C-$NiCo_2O_4$ nanofibers for tunable microwave absorption. Carbon, 2021, 171: 953–962
12 Wang XX, Cao WQ, Cao MS, *et al.* Assembling nano-microarchitecture for electromagnetic absorbers and smart devices. Adv Mater, 2020, 32: 2002112
13 Liu J, Jia Z, Zhou W, *et al.* Self-assembled MoS_2/magnetic ferrite $CuFe_2O_4$ nanocomposite for high-efficiency microwave absorption. Chem Eng J, 2022, 429: 132253
14 Tang Y, Yin P, Zhang L, *et al.* Novel carbon encapsulated zinc ferrite/MWCNTs composite: Preparation and low-frequency microwave absorption investigation. Ceramics Int, 2020, 46: 28250–28261
15 Wahaab FA, Adebayo LL. Electromagnetic properties of Cr-substituted nickel ferrite nanoparticles and their microwave absorption performance. Ceramics Int, 2020, 46: 28506–28513
16 Zhao B, Ma C, Liang L, *et al.* An impedance match method used to tune the electromagnetic wave absorption properties of hierarchical ZnO assembled by porous nanosheets. CrystEngComm, 2017, 19: 3640–3648
17 Xu D, Yang Y, Lyu L, *et al.* One-dimensional MnO@N-doped carbon nanotubes as robust dielectric loss electromagnetic wave absorbers. Chem Eng J, 2021, 410: 128295
18 Xia T, Zhang C, Oyler NA, *et al.* Hydrogenated TiO_2 nanocrystals: A novel microwave absorbing material. Adv Mater, 2013, 25: 6905–6910
19 Xu D, Yang Y, Le K, *et al.* Bifunctional Cu_9S_5/C octahedral composites for electromagnetic wave absorption and supercapacitor applications. Chem Eng J, 2021, 417: 129350
20 Guan XH, Qu P, Guan X, *et al.* Hydrothermal synthesis of hierarchical CuS/ZnS nanocomposites and their photocatalytic and microwave absorption properties. RSC Adv, 2014, 4: 15579–15585
21 Luo J, Hu Y, Xiao L, *et al.* Synthesis of 3D flower-like Fe_3S_4 microspheres and quasi-sphere Fe_3S_4-RGO hybrid-architectures with enhanced electromagnetic wave absorption. Nanotechnology, 2020, 31: 085708
22 Huang B, Wang Z, Hu H, *et al.* Enhancement of the microwave absorption properties of PyC-SiCf/SiC composites by electrophoretic deposition of SiC nanowires on SiC fibers. Ceramics Int, 2020, 46: 9303–9310
23 Li X, Wei J, Chen B, *et al.* Effective electromagnetic wave absorption and photoluminescence performances of flexible SiC nanowires membrane. Ceramics Int, 2021, 47: 17615–17626
24 Zhang Z, Cai Z, Zhang Y, *et al.* The recent progress of MXene-based microwave absorption materials. Carbon, 2021, 174: 484–499
25 Jiang L, Wang Z, Geng D, *et al.* Structure and electromagnetic properties of both regular and defective onion-like carbon nanoparticles. Carbon, 2015, 95: 910–918
26 Qiang R, Du Y, Wang Y, *et al.* Rational design of yolk-shell C@C microspheres for the effective enhancement in microwave absorption. Carbon, 2016, 98: 599–606
27 Fu J, Yang W, Hou L, *et al.* Enhanced electromagnetic microwave absorption performance of lightweight bowl-like carbon nanoparticles. Ind Eng Chem Res, 2017, 56: 11460–11466
28 Ye Z, Li Z, Roberts JA, *et al.* Electromagnetic wave absorption properties of carbon nanotubes-epoxy composites at microwave frequencies. J Appl Phys, 2010, 108: 054315
29 Qi X, Yang Y, Zhong W, *et al.* Large-scale synthesis, characterization and microwave absorption properties of carbon nanotubes of different helicities. J Solid State Chem, 2009, 182: 2691–2697
30 Kong L, Yin X, Zhang Y, *et al.* Electromagnetic wave absorption properties of reduced graphene oxide modified by maghemite colloidal nanoparticle clusters. J Phys Chem C, 2013, 117: 19701–19711
31 Yu H, Wang T, Wen B, *et al.* Graphene/polyaniline nanorod arrays: Synthesis and excellent electromagnetic absorption properties. J Mater Chem, 2012, 22: 21679–21685
32 Liu W, Li H, Zeng Q, *et al.* Fabrication of ultralight three-dimensional graphene networks with strong electromagnetic wave absorption properties. J Mater Chem A, 2015, 3: 3739–3747
33 Shi Y, Gao X, Qiu J. Synthesis and strengthened microwave absorption properties of three-dimensional porous Fe_3O_4/graphene composite foam. Ceramics Int, 2019, 45: 3126–3132
34 Guan H, Wang H, Zhang Y, *et al.* Microwave absorption performance of $Ni(OH)_2$ decorating biomass carbon composites from jackfruit peel. Appl Surf Sci, 2018, 447: 261–268
35 Gao S, An Q, Xiao Z, *et al.* Significant promotion of porous architecture and magnetic Fe_3O_4 NPs inside honeycomb-like carbonaceous composites for enhanced microwave absorption. RSC Adv, 2018, 8: 19011–19023
36 Li Q, Zhang Z, Qi L, *et al.* Toward the application of high frequency electromagnetic wave absorption by carbon nanostructures. Adv Sci, 2019, 6: 1801057
37 Tang J, Bi S, Wang X, *et al.* Excellent microwave absorption of carbon black/reduced graphene oxide composite with low loading. J Mater Sci, 2019, 54: 13990–14001
38 Wang Z, Wei R, Gu J, *et al.* Ultralight, highly compressible and fire-retardant graphene aerogel with self-adjustable electromagnetic wave absorption. Carbon, 2018, 139: 1126–1135
39 Zhang Z, Wang S, Lv Y, *et al.* MnO_2 nanostructures deposited on graphene foams for broadband and lightweight electromagnetic absorption. J Alloys Compd, 2019, 810: 151744
40 Kuang B, Ning M, Wang L, *et al.* Biopolymer nanofiber/reduced

graphene oxide aerogels for tunable and broadband high-performance microwave absorption. Compos Part B-Eng, 2019, 161: 1–9
41 Zhang X, Qiao J, Wang F, *et al.* Tailoring electromagnetic absorption performances of TiO_2/CO/carbon nanofibers through tuning graphitization degrees. Ceramics Int, 2020, 46: 4754–4761
42 Quan B, Shi W, Ong SJH, *et al.* Defect engineering in two common types of dielectric materials for electromagnetic absorption applications. Adv Funct Mater, 2019, 29: 1901236
43 Wen B, Cao MS, Hou ZL, *et al.* Temperature dependent microwave attenuation behavior for carbon-nanotube/silica composites. Carbon, 2013, 65: 124–139
44 Kittel C. On the theory of ferromagnetic resonance absorption. Phys Rev, 1948, 73: 155–161
45 Qiao J, Zhang X, Liu C, *et al.* Facile fabrication of Ni embedded TiO_2/C core-shell ternary nanofibers with multicomponent functional synergy for efficient electromagnetic wave absorption. Compos Part B-Eng, 2020, 200: 108343
46 Wang Y, Li X, Han X, *et al.* Ternary Mo_2C/Co/C composites with enhanced electromagnetic waves absorption. Chem Eng J, 2020, 387: 124159
47 Wu N, Xu D, Wang Z, *et al.* Achieving superior electromagnetic wave absorbers through the novel metal-organic frameworks derived magnetic porous carbon nanorods. Carbon, 2019, 145: 433–444
48 Cao M, Wang X, Cao W, *et al.* Thermally driven transport and relaxation switching self-powered electromagnetic energy conversion. Small, 2018, 14: 1800987
49 Wang XX, Zhang M, Shu JC, *et al.* Thermally-tailoring dielectric "genes" in graphene-based heterostructure to manipulate electromagnetic response. Carbon, 2021, 184: 136–145
50 Shi K, Li J, He S, *et al.* A superior microwave absorption material: Ni^{2+}-Zr^{4+} co-doped barium ferrite ceramics with large reflection loss and broad bandwidth. Curr Appl Phys, 2019, 19: 842–848
51 Wei W, Liu X, Lu W, *et al.* Light-weight gadolinium hydroxide@polypyrrole rare-earth nanocomposites with tunable and broadband electromagnetic wave absorption. ACS Appl Mater Interfaces, 2019, 11: 12752–12760
52 Wang H, Xiang L, Wei W, *et al.* Efficient and lightweight electromagnetic wave absorber derived from metal organic framework-encapsulated cobalt nanoparticles. ACS Appl Mater Interfaces, 2017, 9: 42102–42110
53 Chen C, Bao S, Zhang B, *et al.* Coupling Fe@Fe_3O_4 nanoparticles with multiple-walled carbon nanotubes with width band electromagnetic absorption performance. Appl Surf Sci, 2019, 467-468: 836–843
54 Cao MS, Song WL, Hou ZL, *et al.* The effects of temperature and frequency on the dielectric properties, electromagnetic interference shielding and microwave-absorption of short carbon fiber/silica composites. Carbon, 2010, 48: 788–796
55 Zhang X, Qiao J, Jiang Y, *et al.* Carbon-based MOF derivatives: Emerging efficient electromagnetic wave absorption agents. Nano-Micro Lett, 2021, 13: 135
56 Zhou Y, Wang N, Muhammad J, *et al.* Graphene nanoflakes with optimized nitrogen doping fabricated by arc discharge as highly efficient absorbers toward microwave absorption. Carbon, 2019, 148: 204–213
57 Singh SK, Akhtar MJ, Kar KK. Hierarchical carbon nanotube-coated carbon fiber: Ultra lightweight, thin, and highly efficient microwave absorber. ACS Appl Mater Interfaces, 2018, 10: 24816–24828
58 Liu L, He P, Zhou K, *et al.* Microwave absorption properties of carbon fibers with carbon coils of different morphologies (double microcoils and single nanocoils) grown on them. J Mater Sci, 2014, 49: 4379–4386
59 Khadour M, Atassi Y, abdallah M. Preparation and characterization of a flexible microwave absorber based on MnNiZn ferrite ($Mn_{0.1}Ni_{0.45}Zn_{0.45}Fe_2O_4$) in a thermoset polyurethane matrix. SN Appl Sci, 2020, 2: 1–2
60 Ma J, Wang X, Cao W, *et al.* A facile fabrication and highly tunable microwave absorption of 3D flower-like Co_3O_4-rGO hybrid-architectures. Chem Eng J, 2018, 339: 487–498
61 Wang L, Xing H, Gao S, *et al.* Porous flower-like NiO@graphene composites with superior microwave absorption properties. J Mater Chem C, 2017, 5: 2005–2014
62 Wen B, Cao M, Lu M, *et al.* Reduced graphene oxides: Light-weight and high-efficiency electromagnetic interference shielding at elevated temperatures. Adv Mater, 2014, 26: 3484–3489
63 González M, Baselga J, Pozuelo J. Modulating the electromagnetic shielding mechanisms by thermal treatment of high porosity graphene aerogels. Carbon, 2019, 147: 27–34
64 Liu P, Zhang Y, Yan J, *et al.* Synthesis of lightweight N-doped graphene foams with open reticular structure for high-efficiency electromagnetic wave absorption. Chem Eng J, 2019, 368: 285–298
65 Li Q, Li S, Liu Q, *et al.* Iodine cation bridged graphene sheets with strengthened interface combination for electromagnetic wave absorption. Carbon, 2021, 183: 100–107
66 Li T, Zhi D, Chen Y, *et al.* Multiaxial electrospun generation of hollow graphene aerogel spheres for broadband high-performance microwave absorption. Nano Res, 2020, 13: 477–484
67 Sun X, Li Y, Huang Y, *et al.* Achieving super broadband electromagnetic absorption by optimizing impedance match of rGO sponge metamaterials. Adv Funct Mater, 2022, 32: 2107508
68 Fang Z, Cao X, Li C, *et al.* Investigation of carbon foams as microwave absorber: Numerical prediction and experimental validation. Carbon, 2006, 44: 3368–3370
69 Chen Y, Zhang H, Zeng G. Tunable and high performance electromagnetic absorber based on ultralight 3D graphene foams with aligned structure. Carbon, 2018, 140: 494–503
70 Shi S, Ren S, Hao S, *et al.* Graphene aerogel induced by ethanol-assisted method for excellent electromagnetic wave absorption. J Mater Sci, 2022, 57: 453–466
71 Huang X, Yu G, Zhang Y, *et al.* Design of cellular structure of graphene aerogels for electromagnetic wave absorption. Chem Eng J, 2021, 426: 131894
72 Zhang Y, Gu J. A perspective for developing polymer-based electromagnetic interference shielding composites. Nano-Micro Lett, 2022, 14: 89
73 Zeng Z, Wu N, Yang W, *et al.* Sustainable-macromolecule-assisted preparation of cross-linked, ultralight, flexible graphene aerogel sensors toward low-frequency strain/pressure to high-frequency vibration sensing. Small, 2022, 18: 2202047
74 Cheng Z, Wang R, Cao Y, *et al.* Interfacial π-π interactions induced ultralight, 300°C-stable, wideband graphene/polyaramid foam for electromagnetic wave absorption in both gigahertz and terahertz bands. ACS Appl Mater Interfaces, 2022, 14: 3218–3232
75 Jiang Q, Liao X, Yang J, *et al.* A two-step process for the preparation of thermoplastic polyurethane/graphene aerogel composite foams with multi-stage networks for electromagnetic shielding. Compos Commun, 2020, 21: 100416
76 Wang XX, Shu JC, Cao WQ, *et al.* Eco-mimetic nanoarchitecture for green EMI shielding. Chem Eng J, 2019, 369: 1068–1077
77 Song P, Ma Z, Qiu H, *et al.* High-efficiency electromagnetic interference shielding of rGO@FeNi/epoxy composites with regular honeycomb structures. Nano-Micro Lett, 2022, 14: 51
78 Wang S, Xu J, Li W, *et al.* Magnetic nanostructures: Rational design and fabrication strategies toward diverse applications. Chem Rev, 2022, 122: 5411–5475
79 Liu Y, Zeng Z, Zheng S, *et al.* Facile manufacturing of Ni/MnO nanoparticle embedded carbon nanocomposite fibers for electromagnetic wave absorption. Compos Part B-Eng, 2022, 235: 109800
80 Yang X, Fan S, Li Y, *et al.* Synchronously improved electromagnetic interference shielding and thermal conductivity for epoxy nanocomposites by constructing 3D copper nanowires/thermally annealed graphene aerogel framework. Compos Part A-Appl Sci Manufacturing, 2020, 128: 105670
81 Li J, Yang S, Jiao P, *et al.* Three-dimensional macroassembly of hybrid C@CoFe nanoparticles/reduced graphene oxide nanosheets towards multifunctional foam. Carbon, 2020, 157: 427–436
82 Wang X, Lu Y, Zhu T, *et al.* $CoFe_2O_4$/N-doped reduced graphene oxide aerogels for high-performance microwave absorption. Chem Eng J, 2020, 388: 124317

83 Wang H, Ma H. Highly enhanced electromagnetic wave absorption bandwidth based on reduced graphene oxide-Fe aerogel composites. Nanotechnology, 2019, 31: 095711
84 Wan Z, Shu R, Zhang J, *et al.* Synthesis of three-dimensional porous nitrogen-doped reduced graphene oxide/multi-walled carbon nanotubes composite aerogel as lightweight and high-performance electromagnetic wave absorbers. Diamond Relat Mater, 2021, 112: 108245
85 Lv H, Li Y, Jia Z, *et al.* Exceptionally porous three-dimensional architectural nanostructure derived from CNTs/graphene aerogel towards the ultra-wideband EM absorption. Compos Part B-Eng, 2020, 196: 108122
86 Shu R, Wan Z, Zhang J, *et al.* Facile design of three-dimensional nitrogen-doped reduced graphene oxide/multi-walled carbon nanotube composite foams as lightweight and highly efficient microwave absorbers. ACS Appl Mater Interfaces, 2020, 12: 4689–4698
87 Liang L, Li Q, Yan X, *et al.* Multifunctional magnetic $Ti_3C_2T_x$ MXene/graphene aerogel with superior electromagnetic wave absorption performance. ACS Nano, 2021, 15: 6622–6632
88 Song Q, Ye F, Kong L, *et al.* Graphene and MXene nanomaterials: Toward high-performance electromagnetic wave absorption in gigahertz band range. Adv Funct Mater, 2020, 30: 2000475
89 Qi F, Wang L, Zhang Y, *et al.* Robust $Ti_3C_2T_x$ MXene/starch derived carbon foam composites for superior EMI shielding and thermal insulation. Mater Today Phys, 2021, 21: 100512
90 Zeng ZH, Wu N, Wei JJ, *et al.* Porous and ultra-flexible crosslinked MXene/polyimide composites for multifunctional electromagnetic interference shielding. Nano-Micro Lett, 2022, 14: 59
91 Cheng JB, Wang YQ, Zhang AN, *et al.* Growing MoO_3-doped WO_3 nanoflakes on rGO aerogel sheets towards superior microwave absorption. Carbon, 2021, 183: 205–215
92 Deng L, Zhang J, Shu R. Fabrication of three-dimensional nitrogen-doped reduced graphene oxide/tin oxide composite aerogels as high-performance electromagnetic wave absorbers. J Colloid Interface Sci, 2021, 602: 282–290
93 Sun F, Liu Q, Xu Y, *et al.* Attapulgite modulated thorny nickel nanowires/graphene aerogel with excellent electromagnetic wave absorption performance. Chem Eng J, 2021, 415: 128976
94 Zhao Y, Zuo X, Guo Y, *et al.* Structural engineering of hierarchical aerogels comprised of multi-dimensional gradient carbon nanoarchitectures for highly efficient microwave absorption. Nano-Micro Lett, 2021, 13: 144
95 Yan W, Lien HL, Koel BE, *et al.* Iron nanoparticles for environmental clean-up: Recent developments and future outlook. Environ Sci-Processes Impacts, 2013, 15: 63–77
96 Zhao H, Cheng Y, Lv H, *et al.* A novel hierarchically porous magnetic carbon derived from biomass for strong lightweight microwave absorption. Carbon, 2019, 142: 245–253
97 Lv W, Wen F, Xiang J, *et al.* Peanut shell derived hard carbon as ultralong cycling anodes for lithium and sodium batteries. Electrochim Acta, 2015, 176: 533–541
98 Wang H, Meng F, Li J, *et al.* Carbonized design of hierarchical porous carbon/Fe_3O_4@Fe derived from loofah sponge to achieve tunable high-performance microwave absorption. ACS Sustain Chem Eng, 2018, 6: 11801–11810
99 Zhou X, Jia Z, Feng A, *et al.* Synthesis of fish skin-derived 3D carbon foams with broadened bandwidth and excellent electromagnetic wave absorption performance. Carbon, 2019, 152: 827–836
100 Yang X, Pang X, Cao M, *et al.* Efficient microwave absorption induced by hierarchical pores of reed-derived ultralight carbon materials. Industrial Crops Products, 2021, 171: 113814
101 Aslam MA, Ding W, ur Rehman S, *et al.* Low cost 3D bio-carbon foams obtained from wheat straw with broadened bandwidth electromagnetic wave absorption performance. Appl Surf Sci, 2021, 543: 148785
102 Gu W, Sheng J, Huang Q, *et al.* Environmentally friendly and multifunctional shaddock peel-based carbon aerogel for thermal-insulation and microwave absorption. Nano-Micro Lett, 2021, 13: 102
103 Wu Z, Meng Z, Yao C, *et al.* Rice husk derived hierarchical porous carbon with lightweight and efficient microwave absorption. Mater Chem Phys, 2022, 275: 125246
104 Wang J, Zhou M, Xie Z, *et al.* Enhanced interfacial polarization of biomass-derived porous carbon with a low radar cross-section. J Colloid Interface Sci, 2022, 612: 146–155
105 Zhou X, Jia Z, Feng A, *et al.* Dependency of tunable electromagnetic wave absorption performance on morphology-controlled 3D porous carbon fabricated by biomass. Compos Commun, 2020, 21: 100404
106 Sun X, Wang Z, Wang S, *et al.* Ultrabroad-band and low-frequency microwave absorption based on activated waxberry metamaterial. Chem Eng J, 2021, 422: 130142
107 Hou Y, Quan J, Su X, *et al.* Carbonized silk fiber mat: A flexible and broadband microwave absorber, and the length effect. ACS Sustain Chem Eng, 2021, 9: 12747–12754
108 Rong H, Gao T, Zhang Y, *et al.* Carbonized fibers with multi-elemental doping and hollow architecture derived from natural cotton for tunable microwave absorption properties. J Alloys Compd, 2021, 884: 161084
109 Huang F, Wang S, Ding W, *et al.* Sulfur-doped biomass-derived hollow carbon microtubes toward excellent microwave absorption performance. J Mater Sci-Mater Electron, 2021, 32: 6260–6268
110 Ji C, Liu Y, Xu J, *et al.* Enhanced microwave absorption properties of biomass-derived carbon decorated with transition metal alloy at improved graphitization degree. J Alloys Compd, 2022, 890: 161834
111 Cui J, Wang X, Huang L, *et al.* Environmentally friendly bark-derived Co-doped porous carbon composites for microwave absorption. Carbon, 2022, 187: 115–125
112 Lou Z, Wang Q, Sun W, *et al.* Regulating lignin content to obtain excellent bamboo-derived electromagnetic wave absorber with thermal stability. Chem Eng J, 2022, 430: 133178
113 Zhou X, Jia Z, Feng A, *et al.* Construction of multiple electromagnetic loss mechanism for enhanced electromagnetic absorption performance of fish scale-derived biomass absorber. Compos Part B-Eng, 2020, 192: 107980
114 Song G, Yang K, Gai L, *et al.* ZIF-67/CMC-derived 3D N-doped hierarchical porous carbon with *in-situ* encapsulated bimetallic sulfide and Ni NPs for synergistic microwave absorption. Compos Part A-Appl Sci Manufacturing, 2021, 149: 106584
115 He Y, Xie P, Li S, *et al.* Multifunctional carbon foam with hollow microspheres and a concave-convex microstructure for adjustable electromagnetic wave absorption and wearable applications. J Mater Chem A, 2021, 9: 25982–25998
116 Xu J, Zhang X, Zhao Z, *et al.* Lightweight, fire-retardant, and anti-compressed honeycombed-like carbon aerogels for thermal management and high-efficiency electromagnetic absorbing properties. Small, 2021, 17: 2102032
117 Motojima S, Noda Y, Hoshiya S, *et al.* Electromagnetic wave absorption property of carbon microcoils in 12–110 GHz region. J Appl Phys, 2003, 94: 2325–2330
118 Zhao S, Gao Z, Chen C, *et al.* Alternate nonmagnetic and magnetic multilayer nanofilms deposited on carbon nanocoils by atomic layer deposition to tune microwave absorption property. Carbon, 2016, 98: 196–203
119 Sun G, Yao K, Liu Z, *et al.* A study on measuring the electromagnetic parameters of chiral materials. J Phys D-Appl Phys, 1998, 31: 2109–2111
120 Zhuang Y, Wen J, Tang N, *et al.* High-temperature ferromagnetism of helical carbon nanotubes. AIP Adv, 2013, 3: 052112
121 Wu F, Yang K, Li Q, *et al.* Biomass-derived 3D magnetic porous carbon fibers with a helical/chiral structure toward superior microwave absorption. Carbon, 2021, 173: 918–931
122 Fang Y, Xue W, Zhao R, *et al.* Effect of nanoporosity on the electromagnetic wave absorption performance in a biomass-templated Fe_3O_4/C composite: A small-angle neutron scattering study. J Mater Chem C, 2020, 8: 319–327
123 Li Z, Li H, Ying T, *et al.* What is the important factor affecting microwave absorption performance in corncob-derived carbon/Ni composites? J Phys D-Appl Phys, 2021, 54: 365005
124 Wang L, Shi X, Zhang J, *et al.* Lightweight and robust rGO/sugarcane derived hybrid carbon foams with outstanding EMI shielding per-

formance. J Mater Sci Tech, 2020, 52: 119–126
125 Wang YY, Zhou ZH, Zhu JL, *et al.* Low-temperature carbonized carbon nanotube/cellulose aerogel for efficient microwave absorption. Compos Part B-Eng, 2021, 220: 108985
126 Bai T, Guo Y, Wang D, *et al.* A resilient and lightweight bacterial cellulose-derived C/rGO aerogel-based electromagnetic wave absorber integrated with multiple functions. J Mater Chem A, 2021, 9: 5566–5577
127 Zhang W, Zhang X, Zheng Y, *et al.* Preparation of polyaniline@MoS_2@Fe_3O_4 nanowires with a wide band and small thickness toward enhancement in microwave absorption. ACS Appl Nano Mater, 2018, 1: 5865–5875
128 Zhang D, Liang S, Chai J, *et al.* Highly effective shielding of electromagnetic waves in MoS_2 nanosheets synthesized by a hydrothermal method. J Phys Chem Solids, 2019, 134: 77–82
129 Dong Y, Zhu X, Pan F, *et al.* Fire-retardant and thermal insulating honeycomb-like NiS_2/SnS_2 nanosheets@3D porous carbon hybrids for high-efficiency electromagnetic wave absorption. Chem Eng J, 2021, 426: 131272
130 Zhang X, Cai L, Xiang Z, *et al.* Hollow CuS microflowers anchored porous carbon composites as lightweight and broadband microwave absorber with flame-retardant and thermal stealth functions. Carbon, 2021, 184: 514–525
131 Huang X, Liu X, Jia Z, *et al.* Synthesis of 3D cerium oxide/porous carbon for enhanced electromagnetic wave absorption performance. Adv Compos Hybrid Mater, 2021, 4: 1398–1412
132 Lyu L, Wang F, Zhang X, *et al.* CuNi alloy/carbon foam nanohybrids as high-performance electromagnetic wave absorbers. Carbon, 2021, 172: 488–496
133 Lyu L, Wang F, Li B, *et al.* Constructing 1T/2H MoS_2 nanosheets/3D carbon foam for high-performance electromagnetic wave absorption. J Colloid Interface Sci, 2021, 586: 613–620
134 Dai S, Cheng Y, Quan B, *et al.* Porous-carbon-based Mo_2C nanocomposites as excellent microwave absorber: A new exploration. Nanoscale, 2018, 10: 6945–6953
135 Liang X, Quan B, Ji G, *et al.* Tunable dielectric performance derived from the metal-organic framework/reduced graphene oxide hybrid with broadband absorption. ACS Sustain Chem Eng, 2017, 5: 10570–10579
136 Zhang X, Tian X, Liu C, *et al.* MnCo-MOF-74 derived porous MnO/Co/C heterogeneous nanocomposites for high-efficiency electromagnetic wave absorption. Carbon, 2022, 194: 257–266
137 Lyu L, Zheng S, Wang F, *et al.* High-performance microwave absorption of MOF-derived Co_3O_4@N-doped carbon anchored on carbon foam. J Colloid Interface Sci, 2021, 602: 197–206
138 Shi HG, Wang T, Cheng JB, *et al.* Ultralow-density carbon foam composites with bean-like Co-embedded carbon nanotube whiskers towards high-performance microwave absorption. J Alloys Compd, 2021, 863: 158090
139 Li B, Mao B, Wang X, *et al.* Novel, hierarchical SiC nanowire-reinforced SiC/carbon foam composites: Lightweight, ultrathin, and highly efficient microwave absorbers. J Alloys Compd, 2020, 829: 154609
140 Zhao Y, Zhang Y, Li R, *et al.* Facile synthesis of ultralight and porous melamine-formaldehyde (MF) resin-derived magnetic graphite-like C_3N_4/carbon foam with electromagnetic wave absorption behavior. Crystals, 2020, 10: 656
141 Lou Z, Li R, Wang P, *et al.* Phenolic foam-derived magnetic carbon foams (MCFs) with tunable electromagnetic wave absorption behavior. Chem Eng J, 2020, 391: 123571
142 Liu P, Gao S, Chen C, *et al.* Vacancies-engineered and heteroatoms-regulated N-doped porous carbon aerogel for ultrahigh microwave absorption. Carbon, 2020, 169: 276–287
143 Ye Z, Wang K, Li X, *et al.* Preparation and characterization of ferrite/carbon aerogel composites for electromagnetic wave absorbing materials. J Alloys Compd, 2022, 893: 162396
144 Liu Y, Fan E, Hou R, *et al.* A simple synthesis of magnetic metal implanted hierarchical porous carbon networks for efficient microwave absorption. J Mater Chem C, 2021, 9: 14866–14875
145 Zhao Y, Lou Z, Wang Q, *et al.* Thermal phase transition controlling electromagnetic wave absorption behavior of PAN fiber derived porous magnetic absorber. J Mater Sci-Mater Electron, 2021, 32: 26007–26020
146 Wang Y, Zhang Y, Tao J, *et al.* $Co_{0.2}Fe_{2.8}O_4$/C composite nanofibers with designable 3D hierarchical architecture for high-performance electromagnetic wave absorption. Ceramics Int, 2021, 47: 23275–23284
147 Qiao J, Zhang X, Liu C, *et al.* Facile synthesis of MnS nanoparticle embedded porous carbon nanocomposite fibers for broadband electromagnetic wave absorption. Carbon, 2022, 191: 525–534
148 Zheng S, Zeng Z, Qiao J, *et al.* Facile preparation of C/MnO/Co nanocomposite fibers for high-performance microwave absorption. Compos Part A-Appl Sci Manufact, 2022, 155: 106814
149 Zhao J, Zhang J, Wang L, *et al.* Fabrication and investigation on ternary heterogeneous MWCNT@TiO_2-C fillers and their silicone rubber wave-absorbing composites. Compos Part A-Appl Sci Manufact, 2020, 129: 105714
150 Cheng Y, Zhao H, Lv H, *et al.* Lightweight and flexible cotton aerogel composites for electromagnetic absorption and shielding applications. Adv Electron Mater, 2020, 6: 1900796
151 Zhao J, Zhang J, Wang L, *et al.* Superior wave-absorbing performances of silicone rubber composites *via* introducing covalently bonded SnO_2@MWCNT absorbent with encapsulation structure. Compos Commun, 2020, 22: 100486
152 Li S, Fan Y, Li X, *et al.* Ultralight hard carbon nanotubes nanofiber foam/epoxy nanocomposites for comprehensive microwave absorption performance. Polym Compos, 2021, 42: 4673–4683
153 Zeng Z, Wang C, Wu T, *et al.* Nanocellulose assisted preparation of ambient dried, large-scale and mechanically robust carbon nanotube foams for electromagnetic interference shielding. J Mater Chem A, 2020, 8: 17969–17979
154 Li K, Sun H, Yuan H, *et al.* Three-dimensional architectures assembled with branched metal nanoparticle-encapsulated nitrogen-doped carbon nanotube arrays for absorption of electromagnetic wave. J Alloys Compd, 2020, 821: 153267
155 Yang L, Yin L, Hong C, *et al.* Strong and thermostable hydrothermal carbon coated 3D needled carbon fiber reinforced silicon-boron carbonitride composites with broadband and tunable high-performance microwave absorption. J Colloid Interface Sci, 2021, 582: 270–282
156 Zhao X, Dong S, Hong C, *et al.* Precursor infiltration and pyrolysis cycle-dependent microwave absorption and mechanical properties of lightweight and antioxidant carbon fiber felts reinforced silicon oxycarbide composites. J Colloid Interface Sci, 2020, 568: 106–116
157 Qian J, Shui A, He C, *et al.* Multifunction properties of SiOC reinforced with carbon fiber and *in-situ* SiC nanowires. Ceramics Int, 2021, 47: 8004–8013
158 Liu P, Zhu C, Gao S, *et al.* N-doped porous carbon nanoplates embedded with CoS_2 vertically anchored on carbon cloths for flexible and ultrahigh microwave absorption. Carbon, 2020, 163: 348–359
159 Yin J, Ma W, Gao Z, *et al.* A model for predicting electromagnetic wave absorption of 3D bidirectional angle-interlock woven fabric. Polym Testing, 2021, 100: 107272
160 Zeng Z, Qiao J, Zhang R, *et al.* Nanocellulose-assisted preparation of electromagnetic interference shielding materials with diversified microstructure. SmartMat, 2022, doi: 10.1002/smm2.1118

Acknowledgements This work was supported by the National Key R&D Program of China (2021YFB3502500), the Natural Science Foundation of Shandong Province (2022HYYQ-014 and ZR2016BM16), the Provincial Key Research and Development Program of Shandong (2019JZZY010312), the New 20 Funded Programs for University of Jinan (2021GXRC036), Shenzhen Municipal Special Fund for Guiding Local Scientific and Technological Development (China 2021Szvup071), the Joint Laboratory Project of Electromagnetic Structure Technology (637-2022-70-F-037), and Qilu Young Scholar Program of Shandong University (31370082163127).

Author contributions Liu J and Zeng Z proposed the topic and outline of

the manuscript; Han M collected the related information and drafted the manuscript; Liu J, Zeng Z, Yang Y, and Liu W gave some valuable comments and polished the manuscript.

Conflict of interest The authors declare that they have no conflict of interest.

Mingrui Han received his master's degree from Shanghai University in 2021. Now he works at Shandong University. His current research interest focuses on electromagnetic wave absorbing materials.

Zhihui Zeng received his PhD degree in materials science and engineering from the National Center for Nanoscience and Technology (NCNST), University of Chinese Academy of Sciences, Beijing, China in 2016. Following his work as a postdoctoral research fellow at Nanyang Technological University, Singapore and Swiss Federal Laboratories for Materials Science and Technology (Empa), he currently works at the School of Materials Science and Engineering, Shandong University, Jinan, China. His research interests include the design, fabrication and application of polymer-based nanocomposites, nanostructured assemblies, and cellular materials.

Jiurong Liu obtained his PhD degree from Osaka University in 2004. Then, he worked as a postdoctoral fellow at UCLA until 2008, before beginning his career as a full professor in materials science at Shandong University. His research interests are the synthesis of hybrid nanomaterials for energy storage and their electromagnetic applications.

三维多孔碳基吸波材料的研究进展

韩明睿[1], 杨云霏[1], 刘伟[2], 曾志辉[1*], 刘久荣[1*]

摘要 随着电磁波(EMW)污染的日益严重, 开发高性能电磁波吸收材料(EWAMs)已成为研究热点. 碳基EWAMs具有优异的物理、化学稳定性和高导电性带来的强介电损耗. 特别是三维(3D)多孔碳基EWAMs在EMW吸收研究领域长盛不衰. 3D多孔结构大大降低了材料的密度, 有利于EMW的多次反射和散射, 优化了阻抗匹配, 因此有望实现"低密度、薄厚度、宽吸收带宽、强吸收"的目标. 在此, 我们首先阐明了相关的理论基础和评价方法. 之后, 我们以材料来源为主线索, 总结了3D多孔碳基EWAMs的最新研究进展, 并突出了其中一些独特而新颖的观点. 最后, 提出了3D多孔碳基EWAMs的挑战和前景, 这将有助于高性能EWAMs的进一步发展.

